



















The S-PLUS Ultra-Short Survey: first data release*

Hélio D. Perottoni^{1,2} , Vinicius M. Placco³ , Felipe Almeida-Fernandes² , Fábio R. Herpich⁴ , Silvia Rossi² , Timothy C. Beers⁵ , Rodolfo Smiljanic¹ , João A. S. Amarante^{6,7} , Guilherme Limberg² , Ariel Werle⁸ , Helio J. Rocha-Pinto⁹ , Leandro Beraldo e Silva¹⁰ , Simone Dafflon¹¹ , Alvaro Alvarez-Candal^{12,13} , Gustavo B Oliveira Schwarz^{2,14} , William Schoenell¹⁵ , Tiago Ribeiro¹⁶ , Antonio Kanaan¹⁷ 

¹ Nicolaus Copernicus Astronomical Center, Polish Academy of Sciences, ul. Bartycka 18, 00-716, Warsaw, Poland
e-mail: hperottoni@gmail.com

² Universidade de São Paulo, Instituto de Astronomia, Geofísica e Ciências Atmosféricas, Departamento de Astronomia, SP 05508-090, São Paulo, Brasil

³ NSF NOIRLab, Tucson, AZ 85719, USA

⁴ Institute of Astronomy, University of Cambridge, Madingley Road, Cambridge, CB3 0HA, UK

⁵ Department of Physics and Astronomy and JINA Center for the Evolution of the Elements, University of Notre Dame, Notre Dame, IN 46556, USA

⁶ Institut de Ciències del Cosmos (ICCUB), Universitat de Barcelona (UB), Martí i Franqués, 1, 08028 Barcelona, Spain

⁷ Visiting Fellow, Jeremiah Horrocks Institute, University of Central Lancashire, Preston, PR1 2HE, UK

⁸ INAF-Osservatorio Astronomico di Padova, Vicolo dell'Osservatorio 5, 35122 Padova, Italy

⁹ Universidade Federal do Rio de Janeiro, Observatório do Valongo, Lad. Pedro Antônio 43, 20080-090, Rio de Janeiro, Brazil

¹⁰ Department of Astronomy & Steward Observatory, University of Arizona, Tucson, AZ, 85721, USA

¹¹ Observatório Nacional, MCTI, Rua Gal. José Cristino 77, Rio de Janeiro, 20921-400, RJ, Brazil

¹² Instituto de Astrofísica de Andalucía, CSIC, Apt 3004, E18080 Granada, Spain

¹³ Instituto de Física Aplicada a las Ciencias y las Tecnologías, Universidad de Alicante, San Vicent del Raspeig, E03080, Alicante, Spain

¹⁴ Universidade Presbiteriana Mackenzie, Rua da Consolação, 930, São Paulo, 01302-907, SP, Brazil

¹⁵ GMTO Corporation 465 N. Halstead Street, Suite 250 Pasadena, CA 91107, USA

¹⁶ Rubin Observatory Project Office, 950 N. Cherry Ave., Tucson, AZ 85719, USA

¹⁷ Departamento de Física, Universidade Federal de Santa Catarina, Florianópolis, SC 88040-900, Brazil

July 9, 2024

ABSTRACT

Context. This paper presents the first public data release of the S-PLUS Ultra-Short Survey (USS), a photometric survey with short exposure times, covering approximately 9300 deg² of the Southern sky. The USS utilizes the Javalambre 12-band magnitude system, including narrow and medium-band and broad-band filters targeting prominent stellar spectral features. The primary objective of the USS is to identify bright, extremely metal-poor (EMP; [Fe/H] ≤ −3) and ultra metal-poor (UMP; [Fe/H] ≤ −4) stars for further analysis using medium- and high-resolution spectroscopy.

Aims. This paper provides an overview of the survey observations, calibration method, data quality, and data products. Additionally, it presents the selection of EMP and UMP candidates.

Methods. The data from the USS were reduced and calibrated using the same methods as presented in the S-PLUS DR2. An additional step was introduced, accounting for the offset between the observed magnitudes off the USS and the predicted magnitudes from the very low-resolution Gaia XP spectra.

Results. This first release contains data for 163 observed fields totaling ~324 deg² along the Celestial Equator. The magnitudes obtained from the USS are well-calibrated, showing a difference of ~15 mmag compared to the predicted magnitudes by the GaiaXPpy toolkit. By combining colors and magnitudes, 140 candidates for EMP or UMP have been identified for follow-up studies.

Conclusions. The S-PLUS USS DR1 is an important milestone in the search for bright metal-poor stars, with magnitudes in the range 10 < r ≤ 14. The USS is an ongoing survey; in the near future, it will provide many more bright metal-poor candidate stars for spectroscopic follow-up.

Key words. Surveys – Techniques: photometric – Methods: data analysis – stars: metal-poor – Galaxy: evolution – Galaxy: formation

1. Introduction

The early Universe was characterized by the lack of heavy elements that were gradually formed through the various

* All USS DR1 data is publicly available through the <https://splus.cloud> service.

nucleosynthetic burning and explosive stages of stellar evolution by different nuclear processes (e.g., Burbidge et al. 1957; Cameron 1957). Its chemical and enrichment history can be better understood by studying the oldest stars with lifetimes sufficiently long to still be found in the Milky Way today. These ancient stars hold in their atmospheres valuable information about the chemical composition of the early Universe and how it evolved to its present-day makeup (Beers & Christlieb 2005; Frebel & Norris 2015). In this context, metal-poor stars play a fundamental role in the study of (i) astrophysical sites for the formation of different elements (Nomoto et al. 2013), (ii) the metal-mixing processes that affect the formation of subsequent stellar generations (e.g., Yang & Krumholz 2012; Petit et al. 2015), (iii) the earliest chemical evolution at high redshift ($z > 20$) (Bromm & Larson 2004; Bromm & Yoshida 2011), and (iv) the assembly history of the Milky Way (Yuan et al. 2020b; Limberg et al. 2021a; Gudin et al. 2021; Shank et al. 2022; da Silva & Smiljanic 2023; Zepeda et al. 2023).

To address these questions, significant efforts have been devoted over the past 50 years to systematically identify very metal-poor (VMP; $[\text{Fe}/\text{H}]^1 \leq -2$), extremely metal-poor (EMP; $[\text{Fe}/\text{H}] \leq -3$), and ultra metal-poor (UMP; $[\text{Fe}/\text{H}] \leq -4$) stars (Beers & Christlieb 2005). Early efforts relied on photographic objective-prism surveys followed up with medium-resolution spectroscopy, such as the HK survey (Beers et al. 1985, 1992) and the Hamburg/ESO survey (Christlieb 2003; Christlieb et al. 2008). Later spectroscopic surveys that provided significant numbers of metal-poor stars include the Sloan Digital Sky Survey (SDSS; York et al. 2000), and its sub-surveys, the Sloan Extension for Galactic Understanding and Evolution (SEGUE; Yanny et al. 2009; Rockosi et al. 2022) and the Apache Point Observatory Galactic Evolution Experiment (APOGEE; Majewski et al. 2017), the Radial Velocity Experiment (RAVE; Steinmetz et al. 2006; Placco et al. 2018), the Large Sky Area Multi-object Fiber Spectroscopic Telescope (LAMOST; Cui et al. 2012; Li et al. 2018), and the GALactic Archaeology with HERMES (GALAH; De Silva et al. 2015).

The numbers of recognized metal-poor stars has recently been boosted (Xu et al. 2022a; Andrae et al. 2023; Lu et al. 2023; Yao et al. 2023) by the use of the Gaia DR3 XP Spectra (Gaia Collaboration et al. 2016, 2023b; De Angeli et al. 2023) and by the use of multi-band photometric surveys, such as the Best & Brightest survey (B&B; Schlaufman & Casey 2014; Placco et al. 2019; Limberg et al. 2021b; Xu et al. 2022b). The use of narrow and medium-band photometry of metallicity-sensitive features such as the SkyMapper Southern Sky Survey (SMSS; Keller et al. 2007; Onken et al. 2019; Chiti et al. 2021; Huang et al. 2022), the Pristine survey (Starkenburg et al. 2017; Martin et al. 2023), the Stellar Abundances and Galactic Evolution Survey (SAGES; Zheng et al. 2018; Fan et al. 2023; Huang et al. 2023), the Javalambre Photometric Local Universe Survey (J-PLUS; Cenarro et al. 2019), and the Southern Photometric Local Universe Survey (S-PLUS; Mendes de Oliveira et al. 2019), have led to an increased success in identifying new metal-poor stars (Da Costa et al. 2019; Galarza et al. 2022; Placco et al. 2022; Yang et al. 2022; Almeida-Fernandes et al. 2023; Placco et al. 2023; Huang et al., in prep.).

The increase in the number of metal-poor stars combined with Gaia data has been crucial to revolutionizing our view of the Milky Way's structure and evolution through Galactic Archaeology (e.g., Helmi 2020). In the Galactic halo, a handful of accretion events have been revealed (Kopelman et al. 2019; Naidu et al. 2020; Malhan et al. 2022) as well as various tidal streams (Malhan et al. 2018; Ibata et al. 2019; Yuan et al. 2020a; Ibata et al. 2021; Dodd et al. 2023; Ibata et al. 2023). Moreover, the Galactic disk system also exhibits a very and extremely metal-poor component of unknown (but possibly primordial) origin (Sestito et al. 2019, 2020; Di Matteo et al. 2020; Carter et al. 2021; Cordoni et al. 2021; Hong et al. 2023; Zhang et al. 2023); see simulation efforts by Sestito et al. (2021), Santistevan et al. (2021), Hirai et al. (2022), and Sotillo-Ramos et al. (2023). Furthermore, an old, metal-poor stellar population corresponding to remnants of the earliest phase of galaxy formation has been identified in the inner parts of the Galaxy (Kruijssen et al. 2019; Horta et al. 2021; Belokurov & Kravtsov 2022; Rix et al. 2022; Xiang & Rix 2022), including the discovery of new EMP stars in the bulge region (Howes et al. 2015, 2016; Arentsen et al. 2020; Reggiani et al. 2020).

In particular, EMP and UMP stars are likely to have originated from pristine gas that was relatively free of heavier elements, providing valuable insights into the initial chemical enrichment and the properties of the first massive Population III stars and their subsequent supernovae (e.g., Bromm & Larson 2004; Iwamoto et al. 2005; Nomoto et al. 2013; Frebel & Norris 2015; Jeon et al. 2021; Koutsouridou et al. 2023). Consequently, the chemical abundance patterns of EMP and UMP stars can place direct constraints on the nature of the first stars formed in the Universe; see also Hartwig et al. (2018, 2019, 2023) and Hansen et al. (2020). Additionally, it has also been shown that more than 80% of the observed UMP stars in the Galaxy are carbon enhanced (e.g., Lee et al. 2013; Placco et al. 2014b; Yoon et al. 2018). These carbon-enhanced metal-poor stars (CEMP; $[\text{C}/\text{Fe}] > +0.7$ and $[\text{Fe}/\text{H}] < -1.0$, see Beers & Christlieb 2005 and Aoki et al. 2007) have sparked a great deal of recent interest.

The EMP and UMP stars are rare (Frebel & Norris 2013). The majority found to date are relatively faint, and present very weak spectral lines, making their detailed abundance analyses through high-spectral resolution observations challenging, time-consuming, and sometimes not even feasible for some wavelength ranges, even with 8-10 meter class telescopes. Therefore, it is highly desirable to identify relatively bright EMP and UMP and CEMP stars in order to obtain their detailed spectra, also including the near-ultraviolet spectral region (Ernandes et al. 2023; Bonifacio 2023), increasing the amount of abundance information that can be obtained, (e.g., Placco et al. 2014a, 2015a; Shejeelammal & Goswami 2024), and thereby better constrain theoretical nucleosynthesis models as well as the initial mass function of the first stars (Umeda & Nomoto 2005; Heger & Woosley 2010; Meynet et al. 2010; Nomoto et al. 2013; Jeon et al. 2021; Koutsouridou et al. 2023).

To address the present dearth of relatively bright EMP and UMP stars, we have developed the S-PLUS Ultra-Short Survey (USS) as a sub-survey of S-PLUS. The USS utilizes exposures that are approximately 1/36th of the nominal values used in the S-PLUS survey (Mendes de Oliveira et al. 2019), covering the same 12 photometric bands, and thereby enable the identification of relatively bright VMP

¹Definition of the abundance of a star (\star) relative to the Sun (\odot): $[A/B] = \log(N_A/N_B)_\star - \log(N_A/N_B)_\odot$, where N_A (N_B) is the number of atoms of element A (B).

and EMP stars (Whitten et al. 2019, 2021). By extending the brightness limit by at least four magnitudes, the USS enables observations of brighter sources compared to other narrow-band surveys by avoiding the saturation limitations of previous surveys. Additionally, the identification of relatively bright EMP and UMP stars opens up the possibility of conducting spectroscopic studies in the near-ultraviolet regime using the Hubble Space Telescope (e.g., Placco et al. 2014b, 2015b; Roederer et al. 2016; Holmbeck et al. 2020; Roederer et al. 2022), while it is still available.

This paper is organized as follows. Section 2 outlines the USS design, implementation, and current observing completion status. Section 3 describes the data reduction and calibration of the USS data, followed by details on Data Release 1 (DR1) in Section 4. Preliminary tests on the search for very low-metallicity stars in the USS DR1 are provided in Section 5. Section 6 presents our conclusions and perspectives for future work.

2. The S-PLUS Ultra-Short Survey

The S-PLUS project, facilitated by the S-PLUS Consortium, was built to be the Southern Hemisphere counterpart of J-PLUS, and is operated in collaboration with the Astronomy Department at the University of São Paulo, Brazil. The S-PLUS survey includes various sub-surveys, one of which is known as the S-PLUS Ultra-Short Survey (USS). The USS is an imaging survey that covers the same area as the overall S-PLUS Main Survey, but with much shorter exposure times. As in the S-PLUS Main survey, USS employs a set of 12 bands (seven narrow and medium-band filters and five broad-band filters) for its observations, enabling comprehensive characterization of objects by imaging them in different regions of the optical spectra, with the narrow and medium-band filters placed on crucial elemental absorption lines. This section provides a concise overview of the instruments and observations involved in the USS.

2.1. Survey Instrumentation

The USS is an imaging survey conducted at the Cerro Tololo Inter-American Observatory in Chile, situated at an altitude of approximately 2200 meters. It employs the same telescope, camera, and filters as the S-PLUS to ensure consistency across the projects.

The dedicated telescope for the USS is called the T80-South (T80S), a 0.826m robotic telescope specifically designed for wide-field optical imaging. Although the telescope is automated using the observatory control system *chimera*², the observing staff has access to tools that display cloud cover, weather conditions, and observing status to monitor the progress of the observations. The camera used in the USS is also controlled by the *chimera* system. This camera is designed to capture wide-field images with dimensions of 1.4 by 1.4 degrees, using a CCD of 9232 × 9216 pixels (see Marin-Franch et al. 2012) and a plate scale of 0.55 arcsec pixel⁻¹. The detector is read out via 16 amplifiers arranged in an array of eight columns and two rows, following the same mode as the S-PLUS Main Survey (see Table 1 of Mendes de Oliveira et al. 2019).

The USS adopts the Javalambre filter system (Cenarro et al. 2019), the same 12 bands that the S-PLUS Main

Table 1. USS filter summary and exposure times.

Filter name	λ_{eff} [Å]	Feature	T_{exp} (s)	Filter name	λ_{eff} [Å]	Feature	T_{exp} (s)
<i>u</i>	3533		20	J0515	5133	Mgb Triplet	5
J0378	3773	[O II], CN	19	<i>r</i>	6251		3
J0395	3940	Ca H+K	10	J0660	6613	H α	24
J0410	4095	H δ	5	<i>i</i>	7670		4
J0430	4292	CH G-band	5	J0861	8607	Ca Triplet	7
<i>g</i>	4758		3	<i>z</i>	8936		5

Survey uses. Of those, seven are narrow and medium-band filters designed to map stellar spectral features, and five are SDSS-like broad-bands *ugriz* filters (see Table 1), allowing for the estimation of stellar parameters such as effective temperature (T_{eff}), surface gravity ($\log g$), and metallicity ([Fe/H]) (Gruel et al. 2012), as well as elemental-abundance estimates for a limited additional number of species (e.g., C, N, Mg, and Ca). Huang et al. (in prep.) provide calibrations that are used for the determination of C and Mg abundance estimates; N and Ca will be added in the near future. For more technical details on the survey instrumentation, see Mendes de Oliveira et al. (2019).

2.2. Survey Design

The USS will cover 9300 deg² of the Southern Hemisphere sky when completed. The survey footprint is shown in Figure 1 and follows exactly the same area as the S-PLUS Main Survey. The USS can be separated into two regions: the fields within the S-PLUS Galactic sub-survey area (represented by gold rings in Figure 1) and regions avoiding the Galactic plane (gray and purple symbols). This distinction is necessary because the region near the Galactic plane is significantly more crowded and requires point spread function (PSF) photometry. However, including these fields is not the focus of this paper; rather, it is a topic for future data releases.

The area included in DR1 is divided into 163 tiles (blue circles) along the Celestial Equator, each measuring 2 deg². USS operations began in October 2018 and are expected to last seven years. At the time of this writing, data has been acquired for 3332 tiles in all the 12 bands (purple circles), which accounts for $\sim 70\%$ completion of the USS observations. The coverage area of the observed fields is much larger than that provided in the USS DR1, which serves as a limited sample used to test and refine the method before applying it to all observed fields.

Each tile was observed in a single epoch and had only one exposure per filter, with a total integration time of 110 seconds per tile. The exposure times of the USS (see Table 1) are approximately 1/36th of those from the S-PLUS Main Survey for each filter. Consequently, the saturation limit of the USS is ~ 10 mag for the *r*-band, or about four magnitudes brighter than for the S-PLUS Main Survey.

Given that the USS was developed to optimize usage of the telescope, the observations were taken during all levels of Moon brightness, with a minimum distance of 40 deg from the Moon. In the USS DR1 the median airmass of the observed fields is ~ 1.28 , with a standard deviation of 0.14 (see Table 2). The current physical limit of the observations is set at an altitude of 35 deg, corresponding to an airmass

²<https://github.com/astroufsc/chimera/>

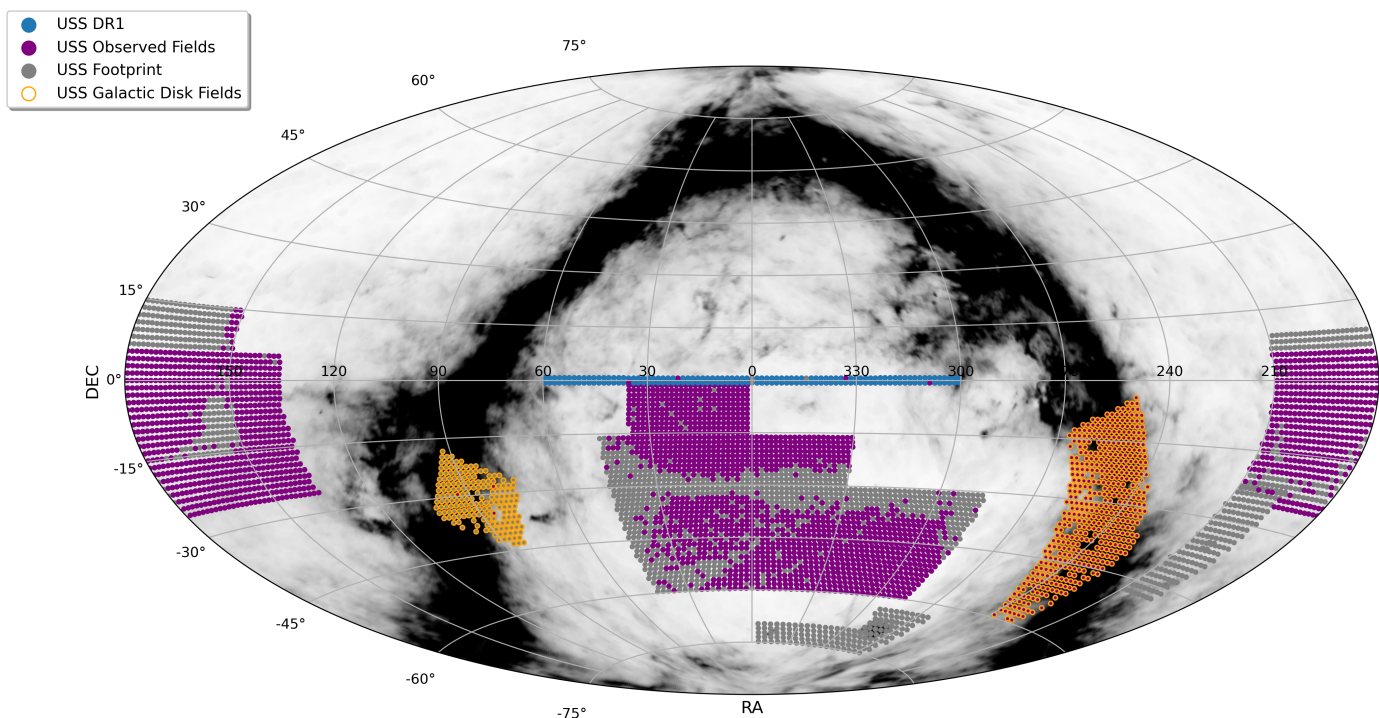


Fig. 1. USS footprint in equatorial coordinates using an Aitoff projection. The blue circles are the USS DR1 fields. The purple circles are the observed fields, and the gold ring indicates the fields in the region of the Galactic disk. The gray circles indicate the footprint area not observed yet. The background represents $E(B - V)$ values ranging from 0.0 (white) to 0.5 (black) according to the map by Schlegel et al. (1998).

Table 2. USS filters mean and standard deviations of the airmass and FWHM spatial coverage.

Filter	Airmass	Airmass	FWHM	FWHM
	Mean	Std	(arcsec) Mean	(arcsec) Std
u	1.28	0.13	1.98	0.60
J0378	1.28	0.13	1.86	0.56
J0395	1.28	0.13	1.80	0.57
J0410	1.28	0.13	1.77	0.57
J0430	1.29	0.14	1.75	0.57
g	1.29	0.14	1.72	0.60
J0515	1.29	0.14	1.68	0.65
r	1.29	0.14	1.42	0.53
J0660	1.29	0.15	1.69	0.58
i	1.29	0.14	1.50	0.53
J0861	1.29	0.15	1.67	0.65
z	1.29	0.15	1.41	0.52

of ~ 1.7 . The fields of the USS that constitute this study point towards regions with low-extinction and present an $\langle E_{(B-V)} \rangle = 0.068$ mag.

3. Calibration Method

The observed images are processed and calibrated similarly to the observations for the S-PLUS Main Survey. Here, we briefly describe this process and the unique procedures used for the USS data.

3.1. Data Reduction and Astrometry

The reduction, comprising overscan and bias subtraction, flat-field correction, and fringe subtraction, uses the same processes as for the Main Survey described in Mendes de Oliveira et al. (2019). The tool deployed is the `jype` pipeline version 0.9.9, the same as used for the S-PLUS data releases to date. The only step of the processing we skip is the co-adding, given that the USS consists of only one observation per filter.

Astrometry is calculated using the SCAMP code (Bertin 2006) and the point source catalog of the Two Micron All Sky Survey (2MASS; Skrutskie et al. 2006) as a reference. We obtain a dispersion of ~ 135 mmas for both RA and DEC, similar to S-PLUS DR2 (Almeida-Fernandes et al. 2022). It is worth noting that being a shallow survey, individual stars can have different sky coordinates compared with other surveys depending on the epoch of the observations due to high proper motion.

3.2. Photometry Extraction

The USS DR1 provides circular aperture photometry obtained using SExtractor (Bertin & Arnouts 1996). The final catalogs contain magnitudes measured in 3- and 6-arcsec diameter apertures (labeled `APER_3` and `APER_6`) and the aperture-corrected instrumental magnitudes (`PStotal`). The `PStotal` apertures correspond to the 3-arcsec apertures, corrected by the amount of flux that the source emits outside this aperture. This correction is obtained by measuring the magnitudes in 32 concentric apertures centered around each source, and computing the average change in magnitude in increasingly larger apertures until the changes converge to

Table 3. Extinction coefficients for the S-PLUS filters.

Filter	λ_{ref} [Å]	k_λ	A_λ/A_V
<i>u</i>	3533.29	4.937	1.593
J0378	3773.13	4.664	1.505
J0395	3940.70	4.480	1.445
J0410	4095.27	4.316	1.392
J0430	4292.39	4.113	1.327
<i>g</i>	4758.49	3.663	1.182
J0515	5133.15	3.334	1.075
<i>r</i>	6251.83	2.515	0.811
J0660	6613.88	2.304	0.743
<i>i</i>	7670.59	1.803	0.582
J0861	8607.59	1.458	0.470
<i>z</i>	8936.64	1.416	0.457

zero. Only sources with a signal-to-noise ratio (S/N) between 30 and 1000 and a CLASS_STAR parameter with a value greater than 0.9 are considered in this step. This correction is computed for every observation in each filter individually, and depends mostly on the atmospheric conditions at the time of the observation (which dictates the seeing and, consequently, the PSF). The PStotal magnitude corresponds to the total magnitude of the source, provided it behaves as a point source in the observation.

3.3. Photometric Calibration Method

In this section, we discuss the techniques applied to perform the photometric calibration of the USS DR1. The PStotal magnitudes used in this section are first corrected for interstellar medium (ISM) extinction using the maps from Schlegel et al. (1998). The magnitudes in the reference catalog are also corrected for ISM extinction in the same way. The extinction coefficients for the S-PLUS filters, which are necessary to correct the ISM extinction, are different from the J-PLUS ones (the coefficients are a function of the transmission curve, which in turn are obtained from the instrument response and atmospheric conditions of the site). To obtain the coefficients, we have used the extinction curve obtained from Schlafly et al. (2016)³, with $R_v = 3.1$. The transmission curves and the reference wavelengths are obtained from the Spanish Virtual Observatory filter profile service⁴; the coefficients for each of the 12 filters are given in Table 3.

The photometric calibration technique applied in the USS takes advantage of the large field of view of the S-PLUS instrument. Each observation contains hundreds of stars with precise photometry and well-known magnitudes in the literature. In this work, for the photometric calibration, we used the reference magnitudes from the ATLAS All-Sky Stellar Reference Catalog (ATLAS Refcat2; Tonry et al. 2018). This catalog provides an almost all-sky coverage with accurate and precise magnitudes for approximately one billion stars down to the AB-magnitude ~ 19 , achieved by compiling the photometry from several surveys, including 2MASS, SMSS, Pan-STARRS DR1 (Chambers

et al. 2016; Flewelling et al. 2020), and Gaia DR2 (Gaia Collaboration et al. 2016, 2018).

The ATLAS Refcat2 provides magnitudes on the Pan-STARRS magnitude system (Chambers et al. 2016). These filters are similar, but not identical, to the filters *g*, *r*, *i*, and *z* in S-PLUS. In addition, the reference catalog does not contain filters similar to the narrow bands. To extract reference magnitudes in the S-PLUS filter system from the data in the reference catalog, we employ the technique presented in Almeida-Fernandes et al. (2022). In summary, this is done by fitting synthetic stellar spectral energy distributions (SEDs) to the reference magnitudes using chi-square minimization. The synthetic SEDs library is obtained by convolving the synthetic spectra from Coelho (2014) with the transmission curves of the reference catalog and the S-PLUS filters.

In practice, the SED fitting process allows us to convert the reference magnitudes in the Pan-STARRS system to reference magnitudes in the S-PLUS system. The calibration zero-points are then obtained by computing the difference between reference and instrumental magnitudes for dozens of stars in each observation. The zero-points are characterized as the mode of the distribution, and since they are estimated using the stars in the science images, they already consider the effects of sky transparency, airmass, and the instrument’s sensitivity for that particular observation.

In the case of the USS, the use of the Refcat2 magnitudes limits the SED-fitting-based calibration to the seven reddest filters, as there is no coverage in the blue range of the spectrum to constrain the models and estimate reliable reference magnitudes for these filters. Therefore, the *u*, J0378, J0395, J0410, and J0430 filters are calibrated using a stellar locus-based technique, also presented in Almeida-Fernandes et al. (2022). In this technique, the stellar locus of the observation in the $y - g \times g - i$ space, where *y* represents a blue filter (with *g* and *i* already previously calibrated), is compared to a reference stellar locus. The difference between the observation and the reference stellar locus is then used to characterize the calibration zero-point for the *y*-band.

After applying the SED-fitting-based calibration for the seven redder filters and the subsequent stellar-locus-based calibration for the five bluer filters, we performed an additional run of the SED-fitting-based calibration. This time, the chi-square minimization is done using the 12 pre-calibrated S-PLUS magnitudes. The use of the 12 filters contributes to better constraining of the synthetic SED models, and was found by Almeida-Fernandes et al. (2022) to improve the calibration by providing corrections on the order of 10 mmag.

3.4. Photometric Quality Assurance

To estimate the accuracy and precision of the photometric calibration, we compared the S-PLUS calibrated magnitudes to the convolved magnitudes obtained from Gaia BP/RP spectra (hereafter XP spectra, Gaia Collaboration et al. 2023a). We obtained the S-PLUS photometry by synthesizing the flux in each S-PLUS filter from the Gaia XP photometry with the GaiaXPY⁵ python library.

³<https://e.schlaf.ly/apored/extcurve.html>

⁴<http://svo2.cab.inta-csic.es/theory/fps/index.php?mode=browse&name=CTIO&name2=S-PLUS&asttype=>

⁵<https://gaia-dpci.github.io/GaiaXPY-website/>

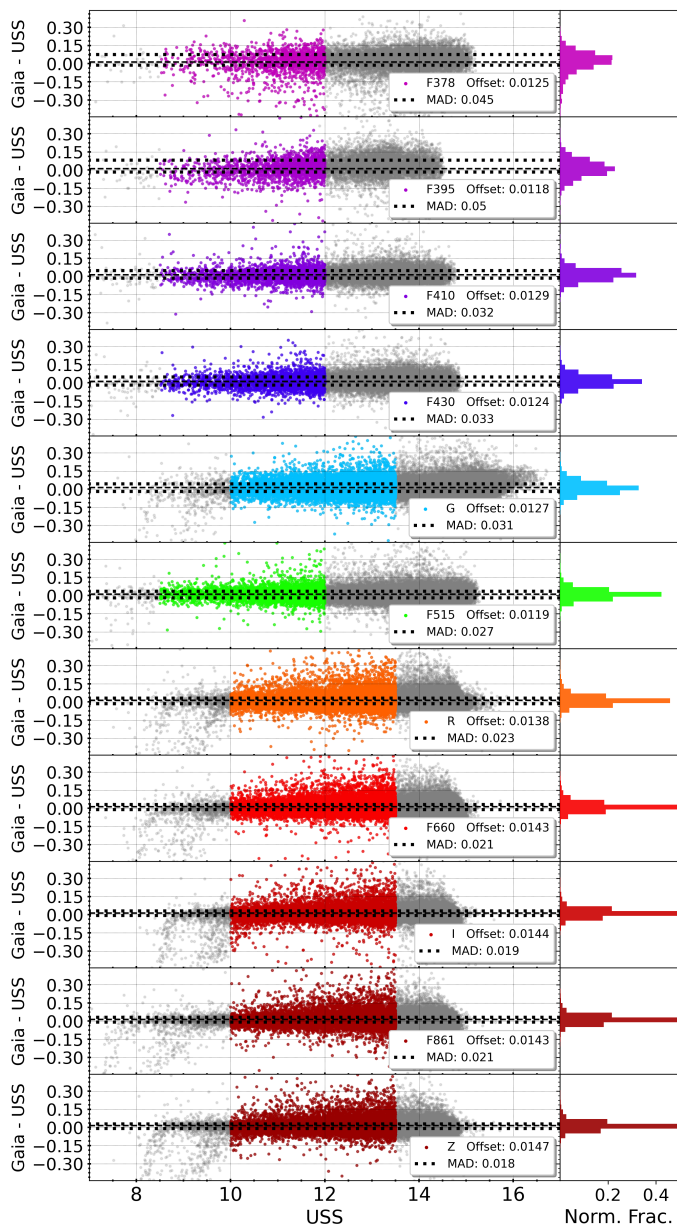


Fig. 2. Residual magnitude differences between S-PLUS magnitudes and the predicted S-PLUS XP spectra magnitudes are presented in each panel, as a function of the S-PLUS magnitudes. The corresponding offset for each filter is indicated in the upper right corner of the respective panel. The colored dots represent the region utilized for offset calculations. The gray dots are the sources with errors smaller than 0.04 mag. The black dotted lines indicate the Mean Absolute Deviation. In the right panels, the normalized fraction of the residual magnitude differences is shown.

The S-PLUS u -band (319.54–384.89 nm) extends beyond the blue edge of the wavelength range covered by Gaia BP/RP spectra of approximately 330 nm. Artificially truncating the u -band at 330 nm may result in significant differences between the observed and predicted magnitudes. To prevent this, we exclusively used eleven S-PLUS filters to compare the observed magnitudes with the predicted S-PLUS XP spectra magnitudes. We will examine comparisons of the calibration with numerical extrapolation tech-

niques, as presented by Xiao et al. (2023) for extrapolating the Gaia XP spectra, in a forthcoming data release.

In addition to the calibration method proposed by Almeida-Fernandes et al. (2022), we introduced a step that considers the offsets between S-PLUS magnitudes and the predicted S-PLUS XP spectra magnitudes. These offsets were then added to the internal step of the photometric calibration. To determine the offset for each filter, we selected objects within a magnitude range to avoid saturation and large photometric errors (< 0.02 mag). For the filters $J0378$, $J0395$, $J0410$, $J0430$, and $J0515$, we selected objects with magnitudes between 8.5 and 12, while for g , r , $J0660$, i , $J0861$, and z , objects within the magnitude range of 10 to 13.5 were considered. This difference arises because the redder filters appear to initiate saturation around 10th mag. As a conservative measure, we are adopting this as the limit regime; the classification of saturated objects will be explored in future data releases.

Figure 2 shows the final calibration accuracy in this work, represented by the residual magnitudes between the S-PLUS magnitudes and the predicted S-PLUS XP spectra magnitudes. The median offset for all filters is 15 mmag, and the average Mean Absolute Deviation (MAD) is 0.026 mag computed using data from the 163 fields in the USS DR1.

4. Photometry Data

This section presents an overview of the data quality in USS DR1. We examine the zero-point distribution, detection completeness to all bands relative to the Gaia DR3 G -band, and the imaging depth achieved at various S/N levels.

4.1. Photometric Magnitude Error

Photometric errors are influenced by factors such as exposure time, weather conditions, and instrument variations over time. Given that photometric conditions in the USS observations are not always ideal, with nights often not meeting the criteria of a dark night (e.g., observations in any moon phase) and good sky transparency (e.g., no clouds or low humidity), a larger dispersion in photometric errors for the same magnitude is expected. This dispersion is further amplified at faint magnitudes due to the smaller number of photons from the source.

Figure 3 shows the photometric magnitude error for USS DR1 data. For bright sources, the photometric errors are negligible over a wide range of magnitudes. The dispersion in the magnitude error data arises primarily from the acquisition under different sky conditions.

Notably, the g , r , and i filters exhibit higher S/N per magnitude, while the filters $J0378$, $J0395$, $J0410$, and $J0430$ display lower S/N, which can be attributed to their respective exposure times. These relationships vary slightly from those in the Main Survey due to the short exposure times, which are only a few seconds, and cannot be further subdivided into smaller values.

It is noteworthy that, for filters with deeper observations, such as g , r , $J0660$, i , $J0861$, and z , brighter sources begin to saturate (see Figure 2). The $J0378$, $J0395$, $J0410$, $J0430$, and $J0515$ filters do not exhibit saturated objects within the same magnitude range.

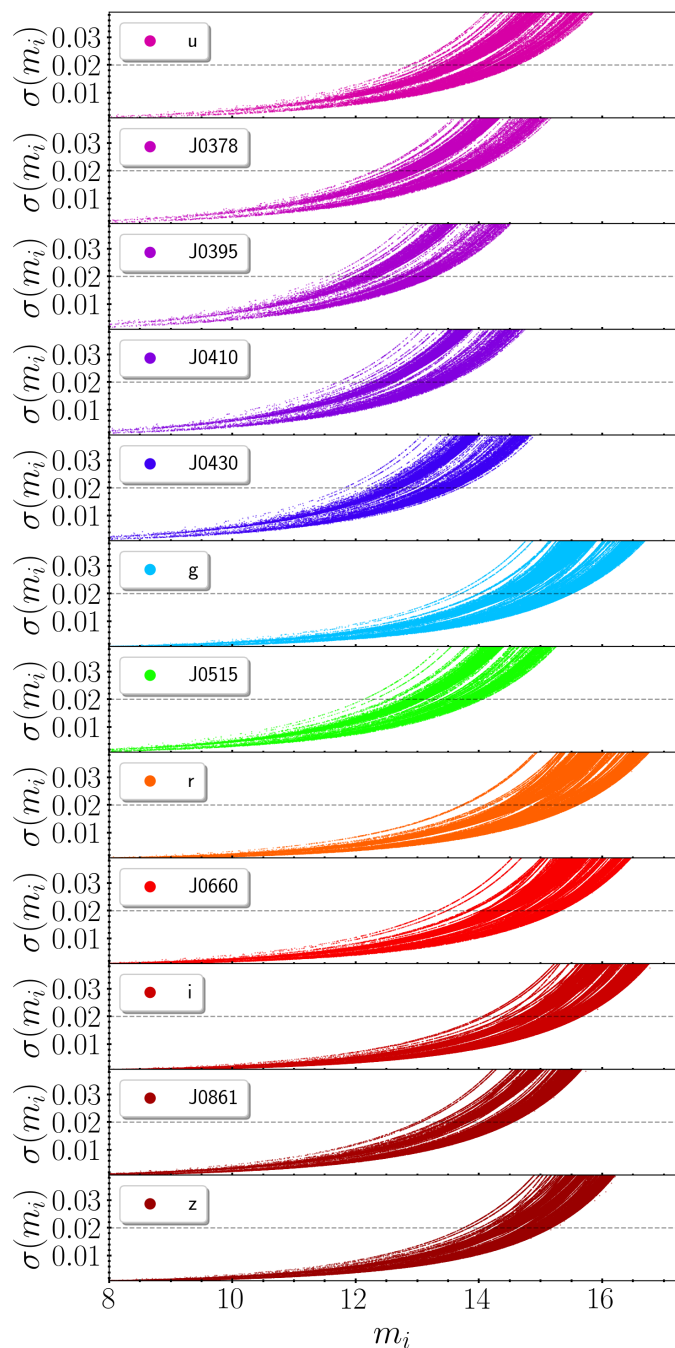


Fig. 3. Photometric error ($\sigma(m_i)$) for each filter (m_i) of the USS. For visual reference, the gray-dashed line indicates where $\sigma(m_i) = 0.02$ mag. The corresponding filter is indicated in the upper left corner of the panel.

While the photometric errors remain around 0.02 mag at magnitude 14 for the filters with deeper observations, a non-negligible photometric error is observed within the same magnitude range for shallower filters. Despite the fact that the redder filters reach a suggested fainter limit for the use of USS DR1 photometry, we explore the data for stars with fainter magnitudes in the subsequent sections.

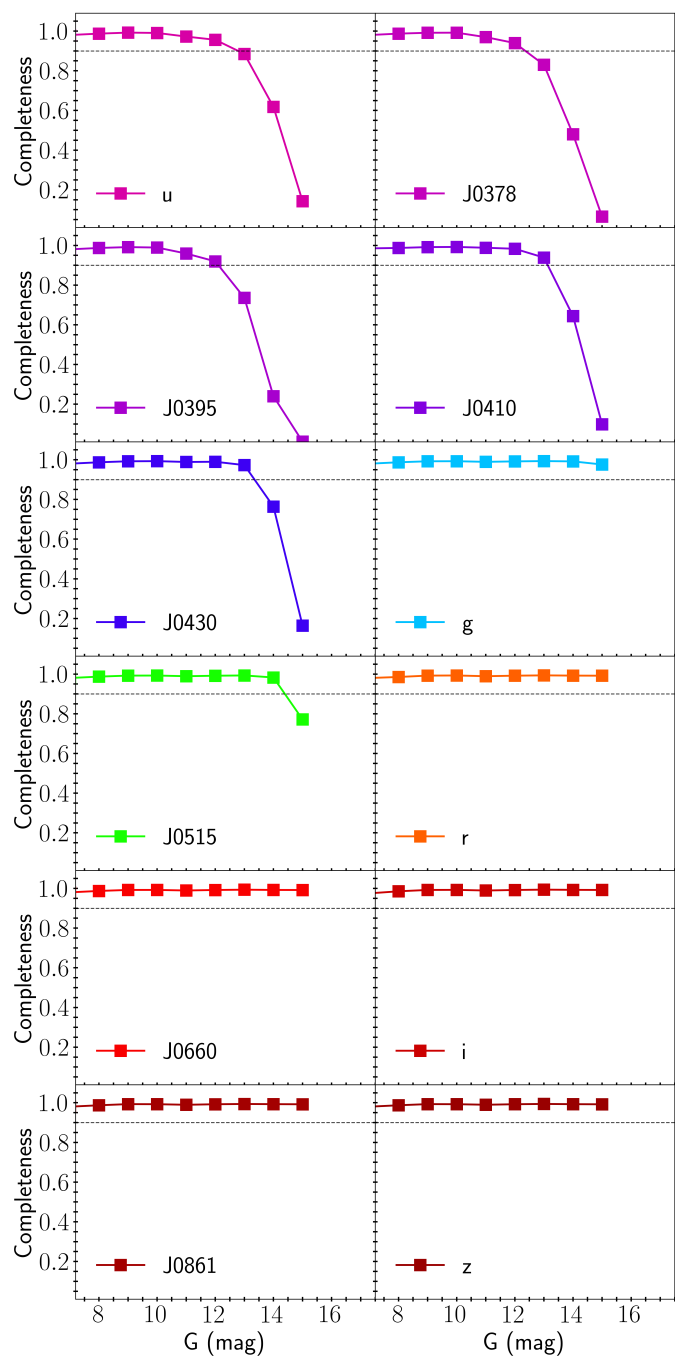


Fig. 4. Detection completeness in relation to the Gaia DR3 G -band for all filters from USS DR1. An internal legend indicates the filters that correspond to each panel. For visual reference, the gray dashed line indicates 90% of sources detected. We considered the detection of all the objects with $S/N > 3$ if the SExtractor attributed a magnitude value other than 99 for this filter.

4.2. Detection Completeness

The detection completeness of the USS filters is determined for the Gaia DR3 G -band for bins of magnitude. Figure 4 shows the average completeness for the 12 bands in relation to the G -band in bins of magnitude. The completeness is around a hundred percent for all bins for the filters g , r , $J0515$, $J0660$, i , $J0861$, and z . For filters u , $J0378$, $J0395$, $J0410$, and $J0430$ the detection completeness reach about

100% until $G < 11$, and decreases significantly for fainter sources. For instance, for some filters, it is not possible to detect approximately 60% of the sources at around $G \sim 14$. This highlights a significant constraint on the use of USS DR1 data.

4.3. Depth

The photometric depths were derived from the PStotal magnitudes of objects observed in the 163 fields from USS DR1. Although this provides a general overview of the depth, for the fainter magnitudes, the errors from the S-PLUS survey are lower than those provided by the USS DR1 due to the observations being taken in better photometric conditions and the co-adding of images.

To obtain these measurements, the photometric depths for the 12 bands were calculated in each field, considering four maximum S/N values (< 10 , < 20 , < 30 , and < 50). For each filter and S/N value, the peak of the magnitude distribution was estimated using a kernel density estimator, applied individually to all fields. Figure 5 shows the distribution of the estimated photometric depths.

4.4. Contents of USS DR1

The S-PLUS website⁶ serves as an interface to access the USS DR1 catalog, and provides a detailed description of the data, documentation of access tools, and example queries in ADQL for the database. Meta-information about object morphology, astrometry, and photometric measurements, along with relevant uncertainties, are presented in the documentation available on the website. It is important to note that the catalog shares the same columns as the single mode from the S-PLUS survey. For a comprehensive description of these columns, the reader may access to the documentation⁷.

The first data release of the USS includes observations of 163 fields, covering a total area of ~ 324 deg², across the 12 bands. The catalog contains approximately 1 million detections, from which $\sim 63,000$ sources have $r < 14$.

5. Search for Metal-Poor Stars

As outlined in the Introduction, EMP and UMP stars play a significant role in addressing various challenges within the fields of Stellar and Galactic Archaeology. The USS offers a valuable opportunity to identify relatively bright low-metallicity stars and conduct spectroscopic analyses to obtain chemical information that is challenging to access with fainter objects. This section describes ongoing efforts to find EMP and UMP candidates for future spectroscopic follow-up programs.

5.1. Data Quality Control Cuts

We performed a series of quality-control cuts on the USS data to ensure the reliable selection of relatively bright EMP and UMP stars. Only sources with a high probability of being a star ($\text{CLASS_STAR_R} \geq 0.90$), not saturated ($\text{SEX_FLAGS_filter} < 4$, for all filters), and with a

precise magnitude estimation ($\text{e_filter_PStotal} \leq 0.2$) were selected. Additionally, we restricted the sample to specific color ranges ($0.2 \leq \text{g_PStotal} - \text{i_PStotal} \leq 1.4$; $0.3 \leq \text{J0410_PStotal} - \text{J0861_PStotal} \leq 3.5$, see Placco et al. 2022) to eliminate potential contamination from white dwarfs and A-type stars at the blue end, and objects cooler than $T_{\text{eff}} \sim 4000$ K (Yanny et al. 2009) at the red end. After applying these criteria, our final sample comprises 45,520 stars. An ADQL query is provided in the Appendix A to retrieve this sample through the S-PLUS website.

5.2. Methodology and Target Selection

In our search for relatively bright EMP and UMP stars, we employ the metallicity- and temperature-sensitive filters available in the USS. In particular, the colors obtained using the narrow-band J0395 filter have proven to be effective in separating different metallicity regimes. The validation of the Javalambre system for estimating stellar metallicity has recently been confirmed through different techniques (Whitten et al. 2019, 2021; Galarza et al. 2022). Moreover, the efficacy of detecting low-metallicity stars using narrow bands has been validated by employing color-color diagrams, which enable the identification of metal-poor stars (Placco et al. 2022; Almeida-Fernandes et al. 2023), leading to the discovery of EMP and UMP stars (Placco et al. 2021, 2023).

Placco et al. (2022), following the work of Starkenburg et al. (2017), selected the color combination (J0395-J0660)-2x(g-i) to distinguish stars in different metallicity regimes. Additionally, Placco et al. (2022) improved the color combination used by Starkenburg et al. (2017) and Da Costa et al. (2019) by employing (J0395-J0410)-(J0660-J0861), which increased the sensitivity to temperature variations. This refined color combination resulted in a success rate of approximately 83% the identification of stars with $[\text{Fe}/\text{H}] < -2.0$. In Figure 6, we select candidates in the aforementioned color-color space by applying the same selection proposed by Placco et al. (2022): (J0395-J0410)-(J0660-J0861) ≤ 0.15 and (J0395-J0660)-2x(g-i) ≤ -0.15 . In this region, we identified a total of 152 stars, from which 91, 25, 7, and 2 targets have r -band magnitudes brighter than 14, 13, 12, and 11, respectively.

Additionally, Placco et al. (2022) observed that a substantial fraction of stars with $[\text{Fe}/\text{H}] > -1.0$ exhibit higher temperatures (i.e., $T_{\text{eff}} > 5900$ K). Taking this into account, Placco et al. (2022) identified a combination of temperature- and metallicity-sensitive filters that can further improve the success rate for identifying stars with $[\text{Fe}/\text{H}] < -2.0$ by removing stars with $T_{\text{eff}} > 5900$ K. Taking this into account, we restricted our target selection to retain only objects that have (J0378-i)-(J0410-J0660) < 0.80 . This resulted in the selection of 140 stars, of which 91, 25, 7, and 2 targets have r -band magnitudes brighter than 14, 13, 12, and 11, respectively.

Placco et al. (2022) and Almeida-Fernandes et al. (2023) have shown that these color selections result in a purity of $\sim 16\%$ for EMP or UMP stars. Assuming a similar metallicity distribution for the magnitude range of the USS DR1, we can expect around 20 relatively bright stars ($r \leq 14$) in our selection of EMP and UMP stars, which translates to 0.4 stars per square degree. The USS is expected to cover an area of 9300 deg² by the end of the survey, resulting in

⁶<https://splus.cloud>

⁷<https://splus.cloud/documentation/uss>

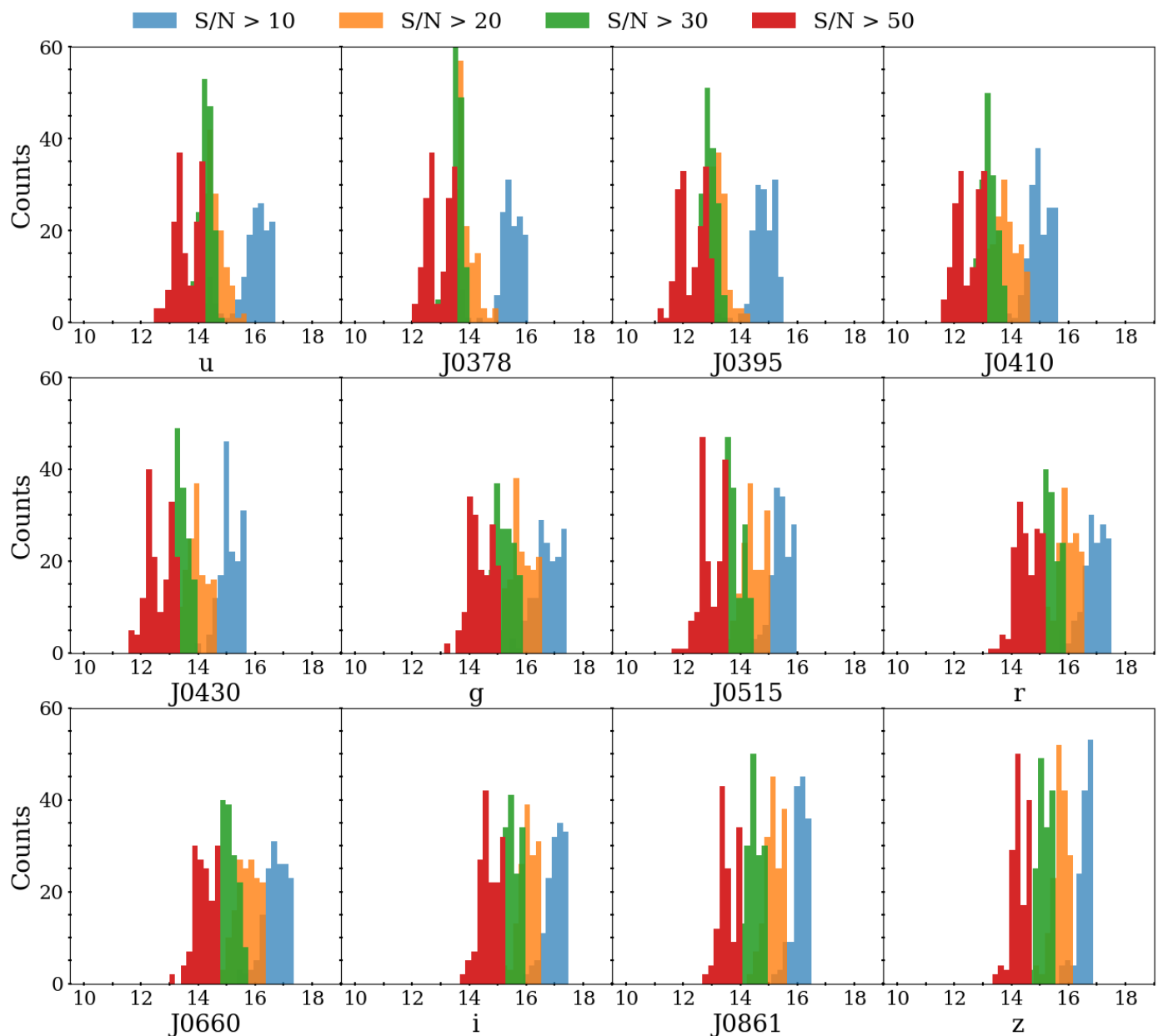


Fig. 5. Photometric depth in PStotal magnitudes for the 12 filters of the USS DR1 for the 163 fields. In the histograms, distinct colors represent different S/N threshold values of 10, 20, 30, and 50, represented in blue, orange, green, and red, respectively.

around 600 relatively bright EMP or UMP stars suitable for high-resolution spectroscopic follow-up.

To compare our selection with photometric metallicities, we opted to use the catalog of [Andrae et al. \(2023\)](#) instead of relying on metal-poor catalogs ([Matsumo et al. 2022](#); [Viswanathan et al. 2023](#); [Yao et al. 2024](#)). Andrae et al. catalog covers a wide range of metallicities and provides insight into the contamination of rich stars in the region. We cross-matched it with our more conservative selection of 140 stars, resulting in 112 stars in common. Within this subset, we observe that 60% are VMP or EMP stars for $r < 13$, and this percentage drops to 50% for $r < 14$. These numbers provide support for the success of our color-based selections, which will continue to provide candidates for spectroscopic follow-up.

6. Conclusion

This paper presents the first data release of the S-PLUS Short Survey (USS), which will cover approximately 9300 deg^2 of the Southern Hemisphere sky. The survey utilizes the Javalambre 12-band magnitude system, including both narrow and medium-band and broad-band filters. This data release contains the data from 163 observed fields, totaling $\sim 324 \text{ deg}^2$ and detecting a total of ~ 1 million sources.

The photometric quality is ensured by a small average offset of 15 mmag between the USS observed magnitudes and those predicted by GaiaXPpy, considering the weather conditions and exposure times. The uncertainties vary, ranging from a few mmag at the bright end to less than 0.02 and ~ 0.04 mag at magnitudes 12 and 14, respectively. We advise caution in using objects brighter than $r = 10$, due to saturation, and objects fainter than $r = 14$, due to

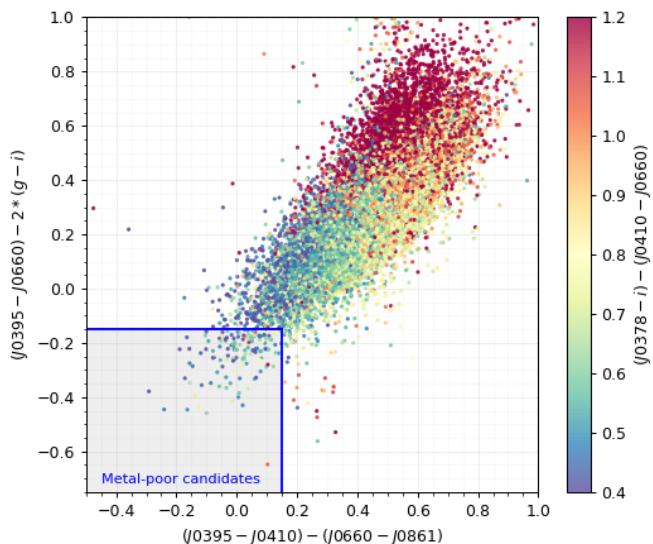


Fig. 6. Selection of low-metallicity stellar candidates in USS DR1, following the criteria proposed by [Placco et al. \(2022\)](#): $(J0395 - J0410) - (J0660 - J0861) \leq 0.15$ and $(J0395 - J0660) - 2x(g - i) \leq -0.15$. The points are color-coded according to the $(J0378 - i) - (J0410 - J0660)$ color; only stars with measurements below 0.8 in this color are included in our final selection.

magnitude errors. In this faint regime, we recommend using data from the S-PLUS Main Survey for more reliable results. We note that the use of the combination of the narrow and medium-band filter fluxes with Gaia BP/RP fluxes (rather than using the broad-band *ugriz* filters, which saturate for stars brighter than $r \sim 10$), can extend our bright limit by several magnitudes, to $r \sim 7 - 8$. Further improvement may be obtained by fitting the wings of the PSFs, and extrapolating to account for the saturated flux, for even brighter stars.

To identify relatively bright EMP and UMP stars within the USS DR1 data, we apply the color-magnitude combinations $((J0395 - J0660) - 2x(g - i))$ and $(J0395 - J0410) - (J0660 - J0861)$ validated by [Placco et al. \(2022\)](#). This method initially flags 152 stars in USS DR1, with 91, 25, 7, and 2 brighter than $r = 14, 13, 12,$ and 11, respectively. A refined selection, incorporating $(J0378 - i) - (J0410 - J0660)$, reduces these numbers to 140 stars, with 84, 23, 6, and 1 brighter than $r = 14, 13, 12,$ and 11, respectively. As estimated by [Placco et al. \(2022\)](#) and [Almeida-Fernandes et al. \(2023\)](#), these strict criteria ensure a purity of approximately 16% for EMP or UMP stars. Extrapolating this to the USS magnitude range, we expect to identify around 20 relatively bright EMP or UMP stars ($r \leq 14$) in DR1, and on the order of 600 stars for subsequent high-resolution spectroscopic follow-up upon the completion of the survey.

Future USS data releases are expected to provide data from thousands of fields. The early scientific exploration of these data will undoubtedly enhance the quality of future USS data releases, particularly with the incorporation of Gaia BP/RP spectra as part of the calibration process. We note that such a procedure has already been carried out for J-PLUS DR3 ([Huang et al., in prep.](#)), and is being finalized for application to S-PLUS DR4. In addition to the determination of stellar parameters (T_{eff} , $\log g$, and $[\text{Fe}/\text{H}]$), these

techniques provide elemental-abundance ratio estimates for $[\text{C}/\text{Fe}]$ and $[\text{Mg}/\text{Fe}]$. Additional elemental-abundance estimates (e.g., $[\text{N}/\text{Fe}]$ and $[\text{Ca}/\text{Fe}]$) will be added in the near future.

Acknowledgements. H.D.P. thanks FAPESP Proc. 2018/21250-9. The work of V.M.P. is supported by NOIRLab, which is managed by the Association of Universities for Research in Astronomy (AURA) under a cooperative agreement with the National Science Foundation. F.A.-F. acknowledges funding for this work from FAPESP (procs 2018/20977-2). F.R.H. acknowledges FAPESP for the financial support via grants 2018/21661-9 and 2021/11345-5. S.R. thanks partial financial support from FAPESP (procs. 2015/50374-0 and 2020/15245-2). T.C.B. acknowledges partial support from grant PHY 14-30152; Physics Frontier Center/JINA Center for the Evolution of the Elements (JINA-CEE), and from OISE-1927130: The International Research Network for Nuclear Astrophysics (IRENA), awarded by the US National Science Foundation. J.A. acknowledges funding from the European Research Council (ERC) under the European Union's Horizon 2020 research and innovation programme (grant agreement No. 852839). G.L. acknowledges FAPESP (proc. 2021/10429-0). A.W. acknowledges funding from the European Research Council (ERC) under the European Union's Horizon 2020 research and innovation program (grant agreement No. 833824, GASP project). L.BeS. acknowledges the support provided by the Heising Simons Foundation through the Barbara Pichardo Future Faculty Fellowship from grant # 2022-3927. S.D. acknowledges CNPq/MCTI for grant 306859/2022-0. A.A.C. acknowledges financial support from the Severo Ochoa grant CEX2021-001131-S funded by MCIN/AEI/10.13039/501100011033. H.D.P. and R.S. acknowledge support from the National Science Centre, Poland, project 2019/34/E/ST9/00133. The S-PLUS project, including the T80-South robotic telescope and the S-PLUS scientific survey was founded as a partnership between the Fundação de Amparo à Pesquisa do Estado de São Paulo (FAPESP), the Observatório Nacional (ON), the Federal University of Sergipe (UFS), and the Federal University of Santa Catarina (UFSC), with important financial and practical contributions from other collaborating institutes in Brazil, Chile (Universidad de La Serena), and Spain (Centro de Estudios de Física del Cosmos de Aragón, CEFCA). We further acknowledge financial support from the São Paulo Research Foundation (FAPESP), Fundação de Amparo à Pesquisa do Estado do RS (FAPERGS), the Brazilian National Research Council (CNPq), the Coordination for the Improvement of Higher Education Personnel (CAPES), the Carlos Chagas Filho Rio de Janeiro State Research Foundation (FAPERJ), and the Brazilian Innovation Agency (FINEP). Members of the S-PLUS collaboration are grateful for the contributions from CTIO staff in helping in the construction, commissioning, and maintenance of the T80-South telescope and camera.

References

- Almeida-Fernandes, F., Placco, V. M., Rocha-Pinto, H. J., et al. 2023, *MNRAS*, 523, 2934
- Almeida-Fernandes, F., SamPedro, L., Herpich, F. R., et al. 2022, *MNRAS*, 511, 4590
- Andrae, R., Rix, H.-W., & Chandra, V. 2023, *ApJS*, 267, 8
- Aoki, W., Beers, T. C., Christlieb, N., et al. 2007, *ApJ*, 655, 492
- Arentsen, A., Starkenburg, E., Martin, N. F., et al. 2020, *MNRAS*, 496, 4964
- Beers, T. C. & Christlieb, N. 2005, *ARA&A*, 43, 531
- Beers, T. C., Preston, G. W., & Shectman, S. A. 1985, *AJ*, 90, 2089
- Beers, T. C., Preston, G. W., & Shectman, S. A. 1992, *AJ*, 103, 1987
- Belokurov, V. & Kravtsov, A. 2022, *MNRAS*, 514, 689
- Bertin, E. 2006, in *Astronomical Society of the Pacific Conference Series*, Vol. 351, *Astronomical Data Analysis Software and Systems XV*, ed. C. Gabriel, C. Arviset, D. Ponz, & S. Enrique, 112
- Bertin, E. & Arnouts, S. 1996, *A&AS*, 117, 393
- Bonifacio, P. 2023, *Experimental Astronomy*, 55, 83
- Bromm, V. & Larson, R. B. 2004, *ARA&A*, 42, 79
- Bromm, V. & Yoshida, N. 2011, *ARA&A*, 49, 373
- Burbidge, E. M., Burbidge, G. R., Fowler, W. A., & Hoyle, F. 1957, *Reviews of Modern Physics*, 29, 547
- Cameron, A. G. W. 1957, *PASP*, 69, 201
- Carter, C., Conroy, C., Zaritsky, D., et al. 2021, *ApJ*, 908, 208
- Cenarro, A. J., Moles, M., Cristóbal-Hornillos, D., et al. 2019, *A&A*, 622, A176

- Chambers, K. C., Magnier, E. A., Metcalfe, N., et al. 2016, arXiv e-prints, arXiv:1612.05560
- Chiti, A., Frebel, A., Mardini, M. K., et al. 2021, *ApJS*, 254, 31
- Christlieb, N. 2003, *Reviews in Modern Astronomy*, 16, 191
- Christlieb, N., Schörck, T., Frebel, A., et al. 2008, *A&A*, 484, 721
- Coelho, P. R. T. 2014, *MNRAS*, 440, 1027
- Cordoni, G., Da Costa, G. S., Yong, D., et al. 2021, *MNRAS*, 503, 2539
- Cui, X.-Q., Zhao, Y.-H., Chu, Y.-Q., et al. 2012, *Research in Astronomy and Astrophysics*, 12, 1197
- Da Costa, G. S., Bessell, M. S., Mackey, A. D., et al. 2019, *MNRAS*, 489, 5900
- da Silva, A. R. & Smiljanic, R. 2023, *A&A*, 677, A74
- De Angeli, F., Weiler, M., Montegriffo, P., et al. 2023, *A&A*, 674, A2
- De Silva, G. M., Freeman, K. C., Bland-Hawthorn, J., et al. 2015, *MNRAS*, 449, 2604
- Di Matteo, P., Spite, M., Haywood, M., et al. 2020, *A&A*, 636, A115
- Dodd, E., Callingham, T. M., Helmi, A., et al. 2023, *A&A*, 670, L2
- Ernandes, H., Barbuy, B., Castilho, B., Evans, C. J., & Cescutti, G. 2023, *Experimental Astronomy*, 55, 149
- Fan, Z., Zhao, G., Wang, W., et al. 2023, *ApJS*, 268, 9
- Flewelling, H. A., Magnier, E. A., Chambers, K. C., et al. 2020, *ApJS*, 251, 7
- Frebel, A. & Norris, J. E. 2013, in *Planets, Stars and Stellar Systems. Volume 5: Galactic Structure and Stellar Populations*, ed. T. D. Oswalt & G. Gilmore, Vol. 5, 55
- Frebel, A. & Norris, J. E. 2015, *ARA&A*, 53, 631
- Gaia Collaboration, Brown, A. G. A., Vallenari, A., et al. 2018, *A&A*, 616, A1
- Gaia Collaboration, Montegriffo, P., Bellazzini, M., et al. 2023a, *A&A*, 674, A33
- Gaia Collaboration, Prusti, T., de Bruijne, J. H. J., et al. 2016, *A&A*, 595, A1
- Gaia Collaboration, Vallenari, A., Brown, A. G. A., et al. 2023b, *A&A*, 674, A1
- Galarza, C. A., Daflon, S., Placco, V. M., et al. 2022, *A&A*, 657, A35
- Gruel, N., Moles, M., Varela, J., et al. 2012, in *Society of Photo-Optical Instrumentation Engineers (SPIE) Conference Series*, Vol. 8448, *Observatory Operations: Strategies, Processes, and Systems IV*, ed. A. B. Peck, R. L. Seaman, & F. Comerón, 84481V
- Gudin, D., Shank, D., Beers, T. C., et al. 2021, *ApJ*, 908, 79
- Hansen, C. J., Koch, A., Mashonkina, L., et al. 2020, *A&A*, 643, A49
- Hartwig, T., Ishigaki, M. N., Klessen, R. S., & Yoshida, N. 2019, *MNRAS*, 482, 1204
- Hartwig, T., Ishigaki, M. N., Kobayashi, C., Tominaga, N., & Nomoto, K. 2023, *ApJ*, 946, 20
- Hartwig, T., Yoshida, N., Magg, M., et al. 2018, *MNRAS*, 478, 1795
- Heger, A. & Woosley, S. E. 2010, *ApJ*, 724, 341
- Helmi, A. 2020, *ARA&A*, 58, 205
- Hirai, Y., Beers, T. C., Chiba, M., et al. 2022, *MNRAS*, 517, 4856
- Holmbeck, E. M., Hansen, T. T., Beers, T. C., et al. 2020, *ApJS*, 249, 30
- Hong, J., Beers, T. C., Lee, Y. S., et al. 2023, arXiv e-prints, arXiv:2311.02297
- Horta, D., Schiavon, R. P., Mackereth, J. T., et al. 2021, *MNRAS*, 500, 1385
- Howes, L. M., Asplund, M., Keller, S. C., et al. 2016, *MNRAS*, 460, 884
- Howes, L. M., Casey, A. R., Asplund, M., et al. 2015, *Nature*, 527, 484
- Huang, Y., Beers, T. C., Wolf, C., et al. 2022, *ApJ*, 925, 164
- Huang, Y., Beers, T. C., Yuan, H., et al. 2023, *ApJ*, 957, 65
- Ibata, R., Malhan, K., Martin, N., et al. 2021, *ApJ*, 914, 123
- Ibata, R., Malhan, K., Tenachi, W., et al. 2023, arXiv e-prints, arXiv:2311.17202
- Ibata, R. A., Malhan, K., & Martin, N. F. 2019, *ApJ*, 872, 152
- Iwamoto, N., Umeda, H., Tominaga, N., Nomoto, K., & Maeda, K. 2005, *Science*, 309, 451
- Jeon, M., Bromm, V., Besla, G., Yoon, J., & Choi, Y. 2021, *MNRAS*, 502, 1
- Keller, S. C., Schmidt, B. P., Bessell, M. S., et al. 2007, *PASA*, 24, 1
- Koppelman, H. H., Helmi, A., Massari, D., Price-Whelan, A. M., & Starkenburg, T. K. 2019, *A&A*, 631, L9
- Koutsouridou, I., Salvadori, S., Skúladóttir, Á., et al. 2023, *MNRAS*, 525, 190
- Kruijssen, J. M. D., Pfeffer, J. L., Reina-Campos, M., Crain, R. A., & Bastian, N. 2019, *MNRAS*, 486, 3180
- Lee, Y. S., Beers, T. C., Masseron, T., et al. 2013, *AJ*, 146, 132
- Li, H., Tan, K., & Zhao, G. 2018, *ApJS*, 238, 16
- Limberg, G., Rossi, S., Beers, T. C., et al. 2021a, *ApJ*, 907, 10
- Limberg, G., Santucci, R. M., Rossi, S., et al. 2021b, *ApJ*, 913, 11
- Lu, X., Yuan, H., Xu, S., et al. 2023, arXiv e-prints, arXiv:2311.16901
- Majewski, S. R., Schiavon, R. P., Frinchaboy, P. M., et al. 2017, *AJ*, 154, 94
- Malhan, K., Ibata, R. A., & Martin, N. F. 2018, *MNRAS*, 481, 3442
- Malhan, K., Ibata, R. A., Sharma, S., et al. 2022, *ApJ*, 926, 107
- Marin-Franch, A., Taylor, K., Cepa, J., et al. 2012, in *Society of Photo-Optical Instrumentation Engineers (SPIE) Conference Series*, Vol. 8446, *Ground-based and Airborne Instrumentation for Astronomy IV*, 84466H
- Martin, N. F., Starkenburg, E., Yuan, Z., et al. 2023, arXiv e-prints, arXiv:2308.01344
- Matsuno, T., Starkenburg, E., Balbinot, E., & Helmi, A. 2022, arXiv e-prints, arXiv:2212.11639
- Mendes de Oliveira, C., Ribeiro, T., Schoenell, W., et al. 2019, *MNRAS*, 489, 241
- Meynet, G., Hirschi, R., Ekstrom, S., et al. 2010, *A&A*, 521, A30
- Naidu, R. P., Conroy, C., Bonaca, A., et al. 2020, *ApJ*, 901, 48
- Nomoto, K., Kobayashi, C., & Tominaga, N. 2013, *ARA&A*, 51, 457
- Onken, C. A., Wolf, C., Bessell, M. S., et al. 2019, *PASA*, 36, e033
- Petit, A. C., Krumholz, M. R., Goldbaum, N. J., & Forbes, J. C. 2015, *MNRAS*, 449, 2588
- Placco, V. M., Almeida-Fernandes, F., Arentsen, A., et al. 2022, *ApJS*, 262, 8
- Placco, V. M., Almeida-Fernandes, F., Holmbeck, E. M., et al. 2023, *ApJ*, 959, 60
- Placco, V. M., Beers, T. C., Ivans, I. I., et al. 2015a, *ApJ*, 812, 109
- Placco, V. M., Beers, T. C., Roederer, I. U., et al. 2014a, *ApJ*, 790, 34
- Placco, V. M., Beers, T. C., Santucci, R. M., et al. 2018, *AJ*, 155, 256
- Placco, V. M., Frebel, A., Beers, T. C., & Stancliffe, R. J. 2014b, *ApJ*, 797, 21
- Placco, V. M., Frebel, A., Lee, Y. S., et al. 2015b, *ApJ*, 809, 136
- Placco, V. M., Roederer, I. U., Lee, Y. S., et al. 2021, *ApJ*, 912, L32
- Placco, V. M., Santucci, R. M., Beers, T. C., et al. 2019, *ApJ*, 870, 122
- Reggiani, H., Schlafman, K. C., Casey, A. R., & Ji, A. P. 2020, *AJ*, 160, 173
- Rix, H.-W., Chandra, V., Andrae, R., et al. 2022, *ApJ*, 941, 45
- Rockosi, C. M., Lee, Y. S., Morrison, H. L., et al. 2022, *ApJS*, 259, 60
- Roederer, I. U., Lawler, J. E., Den Hartog, E. A., et al. 2022, *ApJS*, 260, 27
- Roederer, I. U., Placco, V. M., & Beers, T. C. 2016, *ApJ*, 824, L19
- Santistevan, I. B., Wetzel, A., Sanderson, R. E., et al. 2021, *MNRAS*, 505, 921
- Schlafly, E. F., Meisner, A. M., Stutz, A. M., et al. 2016, *ApJ*, 821, 78
- Schlafman, K. C. & Casey, A. R. 2014, *ApJ*, 797, 13
- Schlegel, D. J., Finkbeiner, D. P., & Davis, M. 1998, *ApJ*, 500, 525
- Sestito, F., Buck, T., Starkenburg, E., et al. 2021, *MNRAS*, 500, 3750
- Sestito, F., Longeard, N., Martin, N. F., et al. 2019, *MNRAS*, 484, 2166
- Sestito, F., Martin, N. F., Starkenburg, E., et al. 2020, *MNRAS*, 497, L7
- Shank, D., Beers, T. C., Placco, V. M., et al. 2022, *ApJ*, 926, 26
- Shejeelammal, J. & Goswami, A. 2024, *MNRAS*, 527, 2323
- Skrutskie, M. F., Cutri, R. M., Stiening, R., et al. 2006, *AJ*, 131, 1163
- Sotillo-Ramos, D., Bergemann, M., Friske, J. K. S., & Pillepich, A. 2023, *MNRAS*, 525, L105
- Starkenburg, E., Martin, N., Youakim, K., et al. 2017, *MNRAS*, 471, 2587
- Steinmetz, M., Zwitter, T., Siebert, A., et al. 2006, *AJ*, 132, 1645
- Tonry, J. L., Denneau, L., Flewelling, H., et al. 2018, *ApJ*, 867, 105
- Umeda, H. & Nomoto, K. 2005, *ApJ*, 619, 427
- Viswanathan, A., Starkenburg, E., Matsuno, T., et al. 2023, arXiv e-prints, arXiv:2309.06137
- Whitten, D. D., Placco, V. M., Beers, T. C., et al. 2021, *ApJ*, 912, 147
- Whitten, D. D., Placco, V. M., Beers, T. C., et al. 2019, *A&A*, 622, A182
- Xiang, M. & Rix, H.-W. 2022, *Nature*, 603, 599
- Xiao, K., Yuan, H., Lopez-Sanjuan, C., et al. 2023, arXiv e-prints, arXiv:2309.11225
- Xu, S., Yuan, H., Niu, Z., et al. 2022a, *ApJS*, 258, 44
- Xu, S., Yuan, H., Zhang, R., et al. 2022b, *ApJS*, 263, 29
- Yang, C.-C. & Krumholz, M. 2012, *ApJ*, 758, 48
- Yang, L., Yuan, H., Xiang, M., et al. 2022, *A&A*, 659, A181
- Yanny, B., Rockosi, C., Newberg, H. J., et al. 2009, *AJ*, 137, 4377
- Yao, Y., Ji, A. P., Kopusov, S. E., & Limberg, G. 2023, arXiv e-prints, arXiv:2303.17676

- Yao, Y., Ji, A. P., Kozlov, S. E., & Limberg, G. 2024, *MNRAS*, 527, 10937
- Yoon, J., Beers, T. C., Dietz, S., et al. 2018, *ApJ*, 861, 146
- York, D. G., Adelman, J., Anderson, John E., J., et al. 2000, *AJ*, 120, 1579
- Yuan, Z., Chang, J., Beers, T. C., & Huang, Y. 2020a, *ApJ*, 898, L37
- Yuan, Z., Myeong, G. C., Beers, T. C., et al. 2020b, *ApJ*, 891, 39
- Zepeda, J., Beers, T. C., Placco, V. M., et al. 2023, *ApJ*, 947, 23
- Zhang, H., Ardern-Arentsen, A., & Belokurov, V. 2023, arXiv e-prints, arXiv:2311.09294
- Zheng, J., Zhao, G., Wang, W., et al. 2018, *Research in Astronomy and Astrophysics*, 18, 147

Appendix A: S-PLUS Cloud Query

The following ADQL query is used to download stars with photometry in all twelve bands of the USS:

```

SELECT
  id, ra, dec,
  r_pstotal, g_pstotal, i_pstotal, z_pstotal, u_pstotal,
  j0378_pstotal, j0395_pstotal, j0410_pstotal,
  j0430_pstotal, j0515_pstotal, j0660_pstotal, j0861_pstotal
FROM
  "usdr1"."usdr1"
WHERE
  class_star_r >= 0.9
  AND sex_flags_r < 4
  AND sex_flags_g < 4
  AND sex_flags_i < 4
  AND sex_flags_u < 4
  AND sex_flags_z < 4
  AND sex_flags_j0378 < 4
  AND sex_flags_j0395 < 4
  AND sex_flags_j0410 < 4
  AND sex_flags_j0430 < 4
  AND sex_flags_j0515 < 4
  AND sex_flags_j0660 < 4
  AND sex_flags_j0861 < 4
  AND e_r_pstotal <= 0.2
  AND e_g_pstotal <= 0.2
  AND e_i_pstotal <= 0.2
  AND e_u_pstotal <= 0.2
  AND e_z_pstotal <= 0.2
  AND e_j0378_pstotal <= 0.2
  AND e_j0395_pstotal <= 0.2
  AND e_j0410_pstotal <= 0.2
  AND e_j0430_pstotal <= 0.2
  AND e_j0515_pstotal <= 0.2
  AND e_j0660_pstotal <= 0.2
  AND e_j0861_pstotal <= 0.2
  AND (g_pstotal - i_pstotal) BETWEEN 0.2 AND 1.4
  AND (j0410_pstotal - j0861_pstotal) BETWEEN 0.3 AND 3.5
  AND r_pstotal != -99 AND g_pstotal != -99 AND i_pstotal != -99
  AND z_pstotal != -99 AND u_pstotal != -99 AND j0378_pstotal != -99
  AND j0395_pstotal != -99 AND j0410_pstotal != -99 AND j0430_pstotal != -99
  AND j0515_pstotal != -99 AND j0660_pstotal != -99 AND j0861_pstotal != -99

```

Appendix B: Catalog of USS DR1 EMP/UMP candidates

Table 4 presents a catalog comprising 140 EMP/UMP candidate stars. The table includes the following columns: ID, RA, DEC and {filter}_PStotal.

Table B.1. Catalog of 140 EMP and UMP candidates

ID	RA (Deg)	DEC (Deg)	<i>r</i>	<i>g</i>	<i>i</i>	<i>z</i>	<i>u</i>	J0378	J0395	J0410	J0430	J0515	J0660	J0861
SDR1_SHORTS-STRIPE82_0004_0000006	1.6576471	1.3953081	13.12	13.59	12.89	12.81	14.55	14.2	14.18	13.92	13.8	13.44	13.05	12.87
SDR1_SHORTS-STRIPE82_0004_0000108	1.1896018	1.0214283	13.41	13.97	13.17	13.09	15.18	14.71	14.66	14.46	14.28	13.78	13.36	13.13
SDR1_SHORTS-STRIPE82_0007_0000510	3.6444336	-0.71293634	13.35	13.96	13.24	12.96	14.53	14.56	14.46	14.27	14.17	13.67	13.29	13.04
SDR1_SHORTS-STRIPE82_0008_0000096	4.5058804	1.0855886	12.94	13.62	12.67	12.52	14.95	14.44	14.43	14.15	13.98	13.4	12.91	12.56
SDR1_SHORTS-STRIPE82_0008_0000210	4.401828	0.15610152	13.92	14.56	13.67	13.55	15.89	15.54	15.16	14.97	14.92	14.33	13.83	13.61
SDR1_SHORTS-STRIPE82_0011_0000366	7.6760125	-1.0947679	13.54	14.14	13.35	13.27	15.13	14.75	14.61	14.41	14.35	13.9	13.49	13.3
SDR1_SHORTS-STRIPE82_0012_0000087	7.4372125	1.1561842	12.63	13.34	12.37	12.25	15.23	14.33	14.07	14.12	13.87	13.15	12.56	12.29
SDR1_SHORTS-STRIPE82_0014_0000254	7.853146	0.20201044	13.76	14.2	13.71	13.66	15.12	14.68	14.47	14.31	14.25	13.86	13.74	13.62
SDR1_SHORTS-STRIPE82_0018_0000370	10.730438	0.23756407	12.14	12.61	11.96	11.91	13.79	13.35	13.2	12.97	12.85	12.45	12.1	11.93
SDR1_SHORTS-STRIPE82_0018_0000459	11.594033	0.44198582	13.96	14.47	13.72	13.61	15.64	15.11	15.0	14.78	14.79	14.25	13.87	13.65
SDR1_SHORTS-STRIPE82_0018_0000464	10.841239	0.4611773	14.47	14.82	14.3	14.35	15.9	15.69	15.23	15.15	15.12	14.7	14.48	14.35
SDR1_SHORTS-STRIPE82_0020_0000462	13.056526	0.35977298	12.42	13.08	12.13	12.01	14.62	14.08	13.95	13.64	13.51	12.88	12.33	12.04
SDR1_SHORTS-STRIPE82_0021_0000446	14.485071	-1.0759861	14.69	15.11	14.6	14.6	16.0	15.78	15.55	15.4	15.27	14.97	14.73	14.58
SDR1_SHORTS-STRIPE82_0023_0000551	16.080364	-0.78245586	14.72	15.37	14.47	14.33	16.68	16.11	16.02	15.8	15.65	15.05	14.66	14.42
SDR1_SHORTS-STRIPE82_0025_0000113	16.50135	-0.30944324	14.32	14.63	14.22	14.2	15.84	15.18	14.89	14.76	14.66	14.54	14.33	14.26
SDR1_SHORTS-STRIPE82_0028_0000295	19.048897	0.7529943	14.53	14.94	14.38	14.32	15.93	15.56	15.24	15.11	15.07	14.66	14.51	14.31
SDR1_SHORTS-STRIPE82_0031_0000252	20.59981	-0.6502333	13.53	14.03	13.42	13.33	14.91	14.74	14.46	14.26	14.24	13.82	13.52	13.34
SDR1_SHORTS-STRIPE82_0033_0000095	21.968967	-0.27128702	14.49	14.77	14.43	14.32	15.53	15.33	14.92	14.98	14.85	14.63	14.45	14.45
SDR1_SHORTS-STRIPE82_0034_0000141	22.496855	0.10427119	13.45	14.01	13.18	13.05	15.22	14.78	14.71	14.33	14.27	13.74	13.38	13.1
SDR1_SHORTS-STRIPE82_0034_0000149	22.547462	0.14666766	10.83	11.2	10.64	10.7	12.23	11.86	11.71	11.45	11.43	11.0	10.8	10.67
SDR1_SHORTS-STRIPE82_0050_0000042	34.65409	1.3091509	14.62	15.05	14.58	14.57	15.9	15.41	15.37	15.22	15.26	14.85	14.69	14.58
SDR1_SHORTS-STRIPE82_0050_0000320	33.967308	0.735502	14.17	14.56	14.02	14.03	15.4	15.06	14.96	14.77	14.78	14.37	14.16	14.01
SDR1_SHORTS-STRIPE82_0051_0000249	35.983967	-1.3795805	14.72	15.24	14.53	14.44	16.17	15.82	15.85	15.58	15.49	14.97	14.64	14.45
SDR1_SHORTS-STRIPE82_0056_0000498	38.236706	0.33034867	14.25	14.93	13.94	13.78	16.58	15.92	15.84	15.58	15.44	14.73	14.16	13.83
SDR1_SHORTS-STRIPE82_0057_0000234	39.839863	-1.2754283	14.62	14.92	14.56	14.6	15.86	15.4	15.14	15.15	14.96	14.71	14.64	14.62
SDR1_SHORTS-STRIPE82_0057_0000248	39.55139	-1.2515044	14.47	14.9	14.36	14.36	15.82	15.59	15.36	15.19	15.15	14.67	14.47	14.32
SDR1_SHORTS-STRIPE82_0062_0000438	43.19201	0.35812354	14.74	15.15	14.59	14.59	16.2	15.94	15.5	15.39	15.34	15.04	14.68	14.56
SDR1_SHORTS-STRIPE82_0072_0000285	49.018974	0.06775388	13.77	14.38	13.59	13.47	15.59	15.07	14.96	14.65	14.55	14.13	13.73	13.51
SDR1_SHORTS-STRIPE82_0074_0000206	50.69091	0.70975673	14.87	15.29	14.7	14.67	16.13	15.93	15.67	15.57	15.51	15.08	14.87	14.69
SDR1_SHORTS-STRIPE82_0079_0000011	54.621475	-0.024894878	14.5	14.93	14.35	14.34	15.82	15.56	15.39	15.23	15.06	14.85	14.49	14.33
SDR1_SHORTS-STRIPE82_0084_0000084	58.519707	1.2353834	13.8	14.41	13.47	13.36	15.52	15.2	15.02	14.93	14.79	14.19	13.73	13.41
SDR1_SHORTS-STRIPE82_0086_0000253	59.402622	0.06786838	14.73	15.43	14.35	14.21	16.95	16.48	16.12	16.08	15.81	15.27	14.59	14.26
SDR1_SHORTS-STRIPE82_0087_0000039	300.19638	-0.03680347	14.86	15.27	14.71	14.68	16.55	15.85	15.58	15.47	15.38	15.12	14.86	14.64
SDR1_SHORTS-STRIPE82_0087_0000408	300.4243	-0.32248077	14.47	14.91	14.28	14.18	15.98	15.74	15.3	15.27	15.22	14.79	14.45	14.23
SDR1_SHORTS-STRIPE82_0087_0001390	301.11063	-0.83181006	13.35	14.01	13.09	12.97	15.49	14.88	14.72	14.4	14.36	13.77	13.28	12.99
SDR1_SHORTS-STRIPE82_0088_0000332	300.17416	1.2281477	14.23	14.92	13.93	13.77	16.61	16.04	15.7	15.52	15.33	14.67	14.16	13.82
SDR1_SHORTS-STRIPE82_0088_0000652	299.81244	1.0351738	14.69	15.15	14.53	14.45	16.51	15.96	15.5	15.56	15.32	14.98	14.67	14.45
SDR1_SHORTS-STRIPE82_0088_0001940	301.00873	0.5642095	14.36	14.92	14.15	14.03	16.26	15.75	15.33	15.32	15.18	14.68	14.3	14.03
SDR1_SHORTS-STRIPE82_0089_0000203	301.38022	-0.20050958	14.24	14.86	14.05	13.98	16.21	15.82	15.41	15.22	15.12	14.55	14.19	14.0
SDR1_SHORTS-STRIPE82_0089_0000227	301.5744	-0.22473826	13.31	13.97	13.02	12.85	15.2	14.8	14.68	14.4	14.32	13.75	13.23	12.91
SDR1_SHORTS-STRIPE82_0089_0000849	301.89993	-1.2271477	14.14	15.5	14.26	13.94	15.81	15.43	15.23	14.82	14.94	14.47	14.6	13.99
SDR1_SHORTS-STRIPE82_0090_0000177	301.85227	1.2722871	13.7	14.38	13.4	13.4	15.9	15.44	15.25	14.93	14.83	14.13	13.66	13.3
SDR1_SHORTS-STRIPE82_0090_0000417	302.25022	1.0935276	13.9	14.51	13.61	13.46	15.85	15.42	15.29	14.93	15.0	14.25	13.83	13.48
SDR1_SHORTS-STRIPE82_0091_0000790	303.37555	-0.62275493	13.07	13.92	12.86	12.94	15.12	14.55	14.31	14.03	13.92	13.38	13.3	12.77

Notes:

The magnitude columns represent values of F_{Stotal} and are not corrected for extinction.

Continued on next page

Table B.1 (continued)

ID	RA (Deg)	DEC (Deg)	<i>r</i>	<i>g</i>	<i>i</i>	<i>z</i>	<i>u</i>	<i>J0378</i>	<i>J0395</i>	<i>J0410</i>	<i>J0430</i>	<i>J0515</i>	<i>J0660</i>	<i>J0861</i>
SDR1_SHORTS-STRIPE82_0092_0000166	303.1313	1.3386507	14.15	14.84	13.8	13.66	16.39	15.73	15.59	15.36	15.27	14.55	14.06	13.72
SDR1_SHORTS-STRIPE82_0092_0000323	303.40805	1.2786375	13.95	14.63	13.64	13.45	16.13	15.45	15.48	15.2	15.01	14.4	13.88	13.53
SDR1_SHORTS-STRIPE82_0092_0002329	303.2324	0.32604828	14.55	15.13	14.24	14.15	16.4	15.99	15.72	15.53	15.48	14.96	14.45	14.16
SDR1_SHORTS-STRIPE82_0092_0003043	302.88132	0.6380521	14.17	14.76	13.89	13.78	16.22	15.79	15.48	15.15	15.08	14.6	14.1	13.79
SDR1_SHORTS-STRIPE82_0093_0000912	305.33347	-1.3431051	14.4	15.03	14.28	14.21	16.42	15.84	15.49	15.35	15.47	14.81	14.39	14.27
SDR1_SHORTS-STRIPE82_0093_0001314	305.38776	-0.5404583	14.35	14.82	14.21	14.14	15.81	15.5	15.21	15.1	15.1	14.61	14.35	14.16
SDR1_SHORTS-STRIPE82_0094_0000946	304.33713	0.07345687	12.92	13.51	12.8	12.73	14.96	14.68	12.61	13.88	13.97	13.32	12.88	12.78
SDR1_SHORTS-STRIPE82_0095_0000790	306.38334	-1.2881083	14.23	14.92	13.98	13.84	16.22	15.98	15.64	15.41	15.32	14.7	14.19	13.87
SDR1_SHORTS-STRIPE82_0095_0001623	306.72748	-0.7906565	11.95	12.69	11.63	11.45	14.1	13.59	13.49	13.15	13.06	12.43	11.85	11.48
SDR1_SHORTS-STRIPE82_0096_0000455	305.97064	1.074333	13.61	14.37	13.25	13.08	16.02	15.38	15.28	14.96	14.74	14.16	13.5	13.11
SDR1_SHORTS-STRIPE82_0098_0000172	307.9158	1.2969278	14.65	15.26	14.45	14.34	16.45	16.26	15.75	15.56	15.62	15.07	14.62	14.34
SDR1_SHORTS-STRIPE82_0098_0000565	308.04758	1.0347829	12.77	13.33	12.56	12.46	14.43	14.01	13.94	13.69	13.59	13.1	12.71	12.46
SDR1_SHORTS-STRIPE82_0098_0000877	307.21344	0.013614895	14.54	15.14	14.28	14.19	16.53	16.17	15.74	15.44	15.47	15.04	14.45	14.22
SDR1_SHORTS-STRIPE82_0099_0000111	309.29166	-0.09919771	14.64	15.05	14.53	14.52	16.19	15.93	15.41	15.4	15.2	14.85	14.64	14.55
SDR1_SHORTS-STRIPE82_0100_0001569	308.3723	0.4099422	14.23	14.8	14.05	13.91	16.01	15.69	15.36	15.16	15.16	14.62	14.21	13.94
SDR1_SHORTS-STRIPE82_0100_0001740	308.47238	0.532722	14.46	14.92	14.34	14.31	16.17	15.86	13.47	15.15	15.15	14.75	14.42	14.32
SDR1_SHORTS-STRIPE82_0101_0000043	310.42578	-0.048552748	14.66	15.06	14.55	14.56	16.07	15.61	15.27	15.34	15.26	14.8	14.67	14.53
SDR1_SHORTS-STRIPE82_0101_0000133	311.02887	-0.15792824	13.64	14.3	13.43	13.28	15.54	15.18	15.05	14.68	14.58	13.99	13.6	13.3
SDR1_SHORTS-STRIPE82_0101_0000211	310.84012	-0.24697165	14.61	14.94	14.52	14.46	15.86	15.7	15.17	15.14	14.92	14.91	14.39	14.05
SDR1_SHORTS-STRIPE82_0101_0000316	310.15854	-0.37324297	14.1	14.62	13.89	13.79	15.66	15.37	15.18	14.92	14.91	14.39	14.05	13.78
SDR1_SHORTS-STRIPE82_0101_0000484	310.93823	-1.3851871	14.06	14.65	14.01	13.96	15.94	15.1	15.02	14.96	14.93	14.49	14.11	13.99
SDR1_SHORTS-STRIPE82_0101_0001249	310.544	-0.70014685	13.94	14.46	13.7	13.61	15.91	15.42	15.16	14.86	14.78	14.22	13.86	13.66
SDR1_SHORTS-STRIPE82_0102_0000839	310.0794	0.16043985	14.07	14.7	13.84	13.74	15.81	15.57	15.4	15.1	15.1	14.52	14.0	13.77
SDR1_SHORTS-STRIPE82_0102_0000916	310.59473	0.8105389	13.74	14.26	13.5	13.37	15.45	14.94	14.77	14.62	14.61	14.1	13.69	13.41
SDR1_SHORTS-STRIPE82_0103_0000736	312.14856	-1.2355337	13.46	14.08	13.2	13.08	15.59	15.13	14.84	14.62	14.43	13.84	13.37	13.12
SDR1_SHORTS-STRIPE82_0104_0000498	312.22162	0.9273911	11.81	12.64	11.46	11.27	14.56	13.9	13.76	13.34	13.16	12.39	11.7	11.31
SDR1_SHORTS-STRIPE82_0104_0001129	311.59122	0.3266088	14.83	15.2	14.67	14.64	16.18	15.85	15.53	15.46	15.43	15.0	14.79	14.63
SDR1_SHORTS-STRIPE82_0104_0001367	311.8505	0.57589555	14.64	15.06	14.5	14.42	16.42	15.7	15.29	15.24	15.25	14.87	14.62	14.44
SDR1_SHORTS-STRIPE82_0104_0001409	312.2212	0.6251173	14.62	15.17	14.45	14.39	16.52	15.93	15.47	15.55	15.44	14.98	14.6	14.39
SDR1_SHORTS-STRIPE82_0104_0001476	312.32614	0.68522644	13.43	14.12	13.17	13.02	15.45	14.91	14.9	14.52	14.44	13.91	13.35	13.05
SDR1_SHORTS-STRIPE82_0105_0000377	313.18854	-0.38996223	13.95	14.47	13.73	13.63	15.54	15.3	15.03	14.78	14.81	14.29	13.89	13.63
SDR1_SHORTS-STRIPE82_0105_0000483	313.69315	-0.49006832	13.77	14.49	13.46	13.29	16.09	15.57	15.39	15.13	15.06	14.24	13.67	13.31
SDR1_SHORTS-STRIPE82_0105_0000549	313.00925	-1.3846456	14.9	15.29	14.78	14.76	16.49	16.19	15.63	15.56	15.6	15.05	14.89	14.78
SDR1_SHORTS-STRIPE82_0105_0000658	312.69165	-1.2699544	13.94	14.34	13.81	13.79	15.1	14.82	14.6	14.57	14.43	14.1	13.89	13.8
SDR1_SHORTS-STRIPE82_0106_0000610	313.1019	0.18768471	13.26	13.94	12.98	12.8	15.32	14.79	14.51	14.42	14.25	13.72	13.17	12.86
SDR1_SHORTS-STRIPE82_0106_0000712	313.80792	0.3431909	14.04	14.68	13.77	13.63	15.99	15.49	15.43	15.13	15.08	14.47	13.98	13.67
SDR1_SHORTS-STRIPE82_0106_0000834	313.8282	0.52028793	13.52	14.18	13.31	13.2	15.55	15.24	14.9	14.61	14.56	13.91	13.46	13.24
SDR1_SHORTS-STRIPE82_0107_0000040	314.83517	-0.388442463	14.32	14.69	14.19	14.11	15.71	15.24	14.86	14.89	14.84	14.55	14.33	14.19
SDR1_SHORTS-STRIPE82_0107_0000253	313.98013	-0.3653406	14.69	15.04	14.58	14.62	16.11	15.86	15.33	15.29	15.2	14.91	14.69	14.64
SDR1_SHORTS-STRIPE82_0107_0000478	315.06863	-1.310828	14.44	14.87	14.3	14.26	15.92	15.48	15.13	15.02	15.0	14.63	14.43	14.32
SDR1_SHORTS-STRIPE82_0107_0000942	314.30426	-0.8858297	14.42	14.8	14.26	14.2	16.16	15.5	15.13	15.08	15.03	14.63	14.38	14.23
SDR1_SHORTS-STRIPE82_0108_0000333	314.37265	1.144085	14.89	15.3	14.78	14.74	16.37	16.11	15.55	15.59	15.44	15.23	14.85	14.76
SDR1_SHORTS-STRIPE82_0108_0000785	314.62006	0.07866466	12.34	13.1	12.0	11.86	14.8	14.29	14.13	13.69	13.56	12.84	12.24	11.89
SDR1_SHORTS-STRIPE82_0108_0000985	314.34805	0.7968035	14.39	14.77	14.27	14.24	15.61	15.44	15.12	15.1	14.98	14.65	14.37	14.26
SDR1_SHORTS-STRIPE82_0108_0001162	314.10263	0.2225285	12.31	14.89	14.01	13.94	13.96	13.75	13.58	13.14	15.13	14.56	14.12	12.13
SDR1_SHORTS-STRIPE82_0108_0001229	314.0349	0.27821594	14.26	14.68	14.12	14.08	15.52	15.32	15.04	15.01	14.9	14.51	14.24	14.07

Notes:

The magnitude columns represent values of PStotal and are not corrected for extinction.

Continued on next page

Table B.1 (continued)

ID	RA (Deg)	DEC (Deg)	r	g	i	z	u	J0378	J0395	J0410	J0430	J0515	J0660	J0861			
SDR1_SHORTS-STRIPE82_0109	0000167	0109	0000167	316.07025	-0.13544065	14.38	15.0	14.18	14.06	16.3	16.02	15.46	15.4	15.22	14.74	14.33	14.08
SDR1_SHORTS-STRIPE82_0109	0000326	0109	0000326	315.71826	-0.28916782	14.01	14.51	13.84	13.81	15.85	15.65	12.52	14.96	14.92	14.32	13.96	13.82
SDR1_SHORTS-STRIPE82_0109	0000535	0109	0000535	316.51276	-0.50278807	14.06	14.62	13.83	13.77	15.65	15.36	15.06	14.88	14.9	14.41	13.99	13.76
SDR1_SHORTS-STRIPE82_0109	0000726	0109	0000726	315.98138	-1.2344275	13.02	13.41	12.83	12.81	14.31	13.96	13.8	13.61	13.57	13.24	12.96	12.82
SDR1_SHORTS-STRIPE82_0109	0000769	0109	0000769	316.11676	-0.8261581	13.95	14.58	13.67	13.53	15.86	15.42	15.14	14.97	14.9	14.32	13.88	13.56
SDR1_SHORTS-STRIPE82_0109	0001384	0109	0001384	316.65747	-0.77296907	14.02	14.61	13.74	13.69	15.85	15.46	15.26	14.97	14.9	14.33	13.91	13.68
SDR1_SHORTS-STRIPE82_0109	0001385	0109	0001385	315.98273	-0.7726212	13.86	14.36	13.68	13.42	15.68	15.34	15.4	15.44	14.71	14.18	14.57	14.45
SDR1_SHORTS-STRIPE82_0109	0001443	0109	0001443	315.9575	-0.71563333	13.78	14.52	13.48	13.33	16.17	15.69	15.39	15.11	14.93	14.26	13.69	13.39
SDR1_SHORTS-STRIPE82_0113	0001171	0113	0001171	319.38544	-0.9063646	13.3	14.06	12.99	12.84	15.8	15.29	15.1	14.68	14.59	13.8	13.2	12.87
SDR1_SHORTS-STRIPE82_0115	0000110	0115	0000110	320.79617	-0.10950566	14.43	14.82	14.26	14.24	16.01	15.49	15.23	15.01	14.94	14.59	14.42	14.29
SDR1_SHORTS-STRIPE82_0116	0000212	0116	0000212	320.9774	1.0159353	14.62	14.95	14.49	14.44	15.87	15.45	15.23	15.28	15.04	14.73	14.6	14.47
SDR1_SHORTS-STRIPE82_0116	0000705	0116	0000705	320.87167	0.46007103	14.38	14.78	14.27	14.21	15.88	15.48	15.06	15.18	14.98	14.59	14.34	14.24
SDR1_SHORTS-STRIPE82_0116	0000832	0116	0000832	320.78775	0.700775	13.44	14.16	13.15	12.99	15.75	15.25	15.04	14.74	14.72	13.88	13.34	13.03
SDR1_SHORTS-STRIPE82_0118	0000130	0118	0000130	321.63882	1.2726451	13.81	14.48	13.55	13.4	15.93	15.32	15.3	14.91	14.81	14.22	13.73	13.39
SDR1_SHORTS-STRIPE82_0119	0000063	0119	0000063	323.6143	-0.1691683	12.32	13.0	12.09	11.96	14.34	13.91	13.71	13.39	13.35	12.76	12.3	12.0
SDR1_SHORTS-STRIPE82_0119	0000096	0119	0000096	323.1112	-0.29941627	14.06	14.54	13.96	13.98	15.59	15.38	14.92	14.8	14.71	14.23	14.08	13.91
SDR1_SHORTS-STRIPE82_0119	0000280	0119	0000280	323.64536	-1.02573	14.24	14.66	14.2	14.17	15.52	15.11	14.79	14.72	14.8	14.48	14.26	14.22
SDR1_SHORTS-STRIPE82_0119	0000315	0119	0000315	323.36276	-0.8233687	11.94	12.77	11.81	11.68	13.91	13.66	13.4	13.28	13.11	12.43	11.81	11.65
SDR1_SHORTS-STRIPE82_0120	0000668	0120	0000668	323.40384	0.3954084	12.03	12.35	11.93	11.9	13.17	12.86	12.61	12.54	12.44	12.2	12.0	11.93
SDR1_SHORTS-STRIPE82_0125	0000766	0125	0000766	327.80646	-0.7942097	13.78	14.35	13.51	13.38	15.49	15.09	14.93	14.78	14.65	14.13	13.7	13.43
SDR1_SHORTS-STRIPE82_0128	0000568	0128	0000568	329.0807	0.19897743	13.55	13.95	13.44	13.41	14.8	14.51	14.29	14.13	14.12	13.81	13.54	13.41
SDR1_SHORTS-STRIPE82_0129	0000049	0129	0000049	330.816	-0.0885891	14.05	14.64	13.85	13.74	15.9	15.47	15.32	15.1	14.95	14.5	14.03	13.76
SDR1_SHORTS-STRIPE82_0131	0000580	0131	0000580	331.396	-0.7343162	13.7	14.38	13.4	13.21	16.04	15.38	15.25	14.93	14.79	14.15	13.6	13.27
SDR1_SHORTS-STRIPE82_0132	0000445	0132	0000445	332.25662	0.8650406	14.39	14.76	14.25	14.26	15.96	15.61	15.12	15.09	14.99	14.73	14.35	14.29
SDR1_SHORTS-STRIPE82_0135	0000179	0135	0000179	334.06198	-0.4520497	14.08	14.6	13.86	13.81	15.94	15.38	15.22	15.19	14.88	14.41	13.99	13.82
SDR1_SHORTS-STRIPE82_0136	0000079	0136	0000079	333.86755	1.2393587	14.91	15.32	14.86	14.79	16.11	16.07	15.56	15.45	15.43	15.21	14.93	14.85
SDR1_SHORTS-STRIPE82_0136	0000384	0136	0000384	334.59164	0.7780391	14.31	14.98	14.0	13.85	16.71	16.08	15.75	15.6	15.36	14.81	14.21	13.87
SDR1_SHORTS-STRIPE82_0139	0000295	0139	0000295	337.55377	-0.88559717	11.66	12.44	11.31	11.15	14.25	13.59	13.48	13.12	12.95	12.22	11.57	11.2
SDR1_SHORTS-STRIPE82_0141	0000013	0141	0000013	338.9892	-0.030445319	14.66	15.06	14.57	14.51	16.28	15.6	15.31	15.25	15.27	14.84	14.65	14.48
SDR1_SHORTS-STRIPE82_0141	0000105	0141	0000105	339.17032	0.2691278	13.21	14.04	12.83	12.67	15.97	15.44	15.19	14.91	14.58	13.75	13.09	12.7
SDR1_SHORTS-STRIPE82_0143	0000035	0143	0000035	339.82462	-0.119511425	13.91	14.55	13.66	13.53	15.81	15.43	15.28	15.14	14.95	14.26	13.85	13.54
SDR1_SHORTS-STRIPE82_0143	0000283	0143	0000283	340.15884	-1.2710394	12.22	13.06	11.86	11.69	14.96	14.33	14.17	13.75	13.59	12.8	12.11	11.74
SDR1_SHORTS-STRIPE82_0147	0000322	0147	0000322	342.71426	-1.0235988	14.7	15.07	14.53	14.48	15.96	15.79	15.49	15.31	15.25	14.92	14.68	14.5
SDR1_SHORTS-STRIPE82_0151	0000121	0151	0000121	346.32645	-0.30182838	13.98	14.37	13.84	13.86	15.58	15.15	14.79	14.7	14.56	14.24	13.95	13.84
SDR1_SHORTS-STRIPE82_0152	0000423	0152	0000423	345.2313	0.21967787	12.38	12.8	12.2	12.23	13.74	13.4	13.27	13.08	13.02	12.68	12.32	12.18
SDR1_SHORTS-STRIPE82_0153	0000034	0153	0000034	346.71744	-0.13730732	12.64	13.21	12.46	12.42	14.28	13.91	13.71	13.51	13.51	12.93	12.59	12.43
SDR1_SHORTS-STRIPE82_0153	0000307	0153	0000307	347.2783	-0.8693464	14.01	14.33	13.82	13.8	15.58	15.15	14.7	14.67	14.62	14.16	13.94	13.88
SDR1_SHORTS-STRIPE82_0154	0000195	0154	0000195	347.83527	0.9204981	14.14	14.58	13.9	13.86	15.89	15.53	15.2	14.98	14.85	14.43	14.06	13.86
SDR1_SHORTS-STRIPE82_0157	0000444	0157	0000444	350.66132	-0.9999145	14.18	14.52	14.07	14.04	15.44	15.06	14.83	14.77	14.68	14.4	14.18	14.06
SDR1_SHORTS-STRIPE82_0160	0000250	0160	0000250	351.24118	0.149503	14.12	14.61	13.98	14.05	15.58	15.32	15.1	15.0	14.77	14.47	14.12	14.04
SDR1_SHORTS-STRIPE82_0160	0000271	0160	0000271	351.37036	0.5066438	13.48	14.21	13.06	12.99	16.15	15.46	15.34	14.95	14.83	14.0	13.36	13.03
SDR1_SHORTS-STRIPE82_0161	0000253	0161	0000253	353.3934	-1.3361326	12.97	13.43	12.88	12.83	14.23	13.98	13.81	13.59	13.56	13.21	12.96	12.85
SDR1_SHORTS-STRIPE82_0161	0000324	0161	0000324	353.44833	-0.5359643	14.34	14.77	14.26	14.21	15.75	15.42	15.08	14.92	14.87	14.58	14.37	14.21
SDR1_SHORTS-STRIPE82_0161	0000438	0161	0000438	353.4584	-0.9787993	14.73	15.18	14.66	14.6	16.23	15.75	15.58	15.4	15.26	15.08	14.78	14.58
SDR1_SHORTS-STRIPE82_0162	0000159	0162	0000159	353.3701	0.9590613	14.0	14.42	13.85	13.78	15.38	15.13	14.87	14.7	14.73	14.21	13.97	13.83

Notes:

The magnitude columns represent values of PStotal and are not corrected for extinction.

Continued on next page

Table B.1 (*continued*)

ID	RA (Deg)	DEC (Deg)	<i>r</i>	<i>g</i>	<i>i</i>	<i>z</i>	<i>u</i>	<i>J0378</i>	<i>J0395</i>	<i>J0410</i>	<i>J0430</i>	<i>J0515</i>	<i>J0660</i>	<i>J0861</i>
SDR1_SHORTS-STRIPE82_0163_0000365	353.72775	-0.95116305	12.64	13.21	12.46	12.37	14.34	13.91	13.87	13.57	13.48	12.99	12.6	12.37
SDR1_SHORTS-STRIPE82_0166_0000308	355.3462	0.28945935	13.84	14.44	13.57	13.44	15.84	15.23	15.19	15.03	14.78	14.3	13.75	13.5
SDR1_SHORTS-STRIPE82_0166_0000317	355.2404	0.34346882	13.44	13.93	13.27	13.21	15.22	14.94	13.01	14.45	14.3	13.78	13.36	13.26
SDR1_SHORTS-STRIPE82_0169_0000403	358.82654	-0.8964953	13.82	14.47	13.61	13.49	15.83	15.33	15.28	14.99	14.82	14.25	13.76	13.53

Notes:

The magnitude columns represent values of P_{Stotal} and are not corrected for extinction.